Tutorials and Reviews

International Journal of Bifurcation and Chaos, Vol. 8, No. 6 (1998) 1053–1093

PATCHINESS: A NEW DIAGNOSTIC FOR LAGRANGIAN TRAJECTORY ANALYSIS IN TIME-DEPENDENT FLUID FLOWS*

NARESH MALHOTRA
Control and Dynamical Systems MC 107-81, Caltech, Pasadena, CA 91125, USA

IGOR MEZIĆ
Mechanical and Environmental Engineering, University of California, Santa Barbara, CA 93106, USA

STEPHEN WIGGINS
Control and Dynamical Systems MC 107-81, Caltech, Pasadena, CA 91125, USA

Received September 26, 1997; Revised June 5, 1998

In 2-D time-dependent fluid flows, a patch represents a localized region in space that has a significantly different average velocity compared to its surroundings. We show that one can obtain important information about the Lagrangian particle motion in such flows by studying the nature, long-term evolution, and statistical characteristics of the patchiness behavior. For example, the dispersion of passive tracers at any time is directly related to the distribution of patches in the flow. We thoroughly investigate the transport properties of the Lagrangian trajectories associated with a cellular flow previously used as a model for time-dependent Rayleigh–Bénard convection, and a kinematic model of a meandering jet (originally due to Bower [1991]). In both cases, we examine the statistical attributes of the patchiness, their relationship with the geometric features of the stable and unstable manifolds, and the effect of noise on the structure of patchiness. We uncover some interesting features associated with the origin of these patches and their influence on Lagrangian transport.

*This research was supported by ONR Grant No. N00014-97-1-0071.

1. Introduction

There has been much work on applying dynamical systems techniques to the study of mixing and transport issues in fluids over the past ten years. Babiano *et al.* [1994] and Aref and El Naschie [1994] provide recent reviews. In two dimensions the analogy between the global, geometrical study of dynamical systems theory and transport of fluid in time-periodic flows is quite apparent. For two-dimensional, incompressible time-periodic fluid flows, the equations for the trajectories of a point in the fluid are given by

$$\begin{aligned} \dot{x} &= \frac{\partial \psi}{\partial y}(x, y, t)\,, \\ \dot{y} &= -\frac{\partial \psi}{\partial x}(x, y, t)\,, \end{aligned} \tag{1}$$

where $\psi(x, y, t)$ is the stream function, periodic in t. These trajectories are also referred to as "fluid particle trajectories". Thus, a fluid "particle" is analogous to the "point" in geometry. In that sense, it is a somewhat fictitious notion, but practically, very useful. A number of physical situations arise where material particles are transported by the flow, yet their presence does not affect the flow. In this case, the trajectories of the material particles in the flow can be considered to be the fluid particle trajectories. We refer to such material as "passive tracers, or scalars" (e.g. the reader can think of dye being placed in a fluid as a passive scalar, or tracer). Transport of material points in a flow is often referred to as *Lagrangian transport* since the formulation of the theory of fluid mechanics in the setting of the material properties of the fluid is referred to as the Lagrangian viewpoint of fluid mechanics. Similarly, fluid particle trajectories are often called "Lagrangian trajectories".

From the dynamical systems viewpoint, these equations for fluid particle trajectories are just Hamilton's equations where $\psi(x, y, t)$ is the Hamiltonian function and the phase space of this dynamical system is actually the physical space where the fluid flows. Through time periodicity the study of these equations can be reduced to the study of a two-dimensional, symplectic Poincaré map and once the problem has been cast in this setting a variety of techniques and ideas from dynamical systems theory can be applied for the purpose of studying fluid transport and mixing issues. For example, KAM tori represent barriers to fluid transport and mixing, chaotic dynamics should act to enhance mixing, and invariant manifolds, such as the stable and unstable manifolds of hyperbolic periodic points, are manifested as "organized structures" in the fluid flow.

One of the advantages of the dynamical systems viewpoint for studying large-scale geometrical structures in fluid flows is that most dynamical systems results are not dependent on a specific analytical form of the dynamical system under consideration. Rather, they require that only certain *geometrical features* be present. For example, the existence of stable and unstable manifolds of some invariant set requires only the existence of a hyperbolic invariant set, the existence of Smale

horseshoe type chaos requires only the transverse intersection of the stable and unstable manifolds of a hyperbolic periodic orbit, and the existence of KAM tori requires only that the flow be a two-dimensional time-quasiperiodic perturbation of an integrable flow that has a region of closed streamlines. If it is known that these structures are present in the flow, then this information, along with information on their geometrical arrangement in the flow, can be used to gain a quantitative understanding of transport. For example, if a flow with periodic boundary conditions contains a KAM torus, then the recent work of Mezić and Wiggins [1995a] shows that, neglecting molecular diffusion, an initial distribution of tracer that is both inside and outside the KAM torus will exhibit asymptotic t^2 dispersion. If the effects of molecular diffusion are considered, then the work of Mezić *et al.* [1996] shows that in the high Peclet number limit the effective diffusivity scales are like the square of the Peclet number. The existence of a Smale horseshoe implies the existence of *local* exponential expansion of fluid line elements and rapid stirring of fluid. The stable and unstable manifolds of hyperbolic periodic orbits may form a template which governs large scale transport in a flow [Beigie *et al.*, 1994]. A common feature of each of these examples is that a "low dimensional" geometric feature of the flow can be used to quantify a more global feature of the transport.

A central topic in this paper is the nature of the distribution of passive scalars in a fluid flow. From the point of view of dynamical systems theory, this is the study of the distribution in phase space of the time evolution of ensembles of initial conditions. Recent studies of the distribution of passive scalars in fluid flows have concentrated on the so-called anomalous diffusion properties of such distributions (see [Shlesinger *et al.*, 1994] and the references therein). These are commonly observed in the regions of physical space where the flow under consideration is mixing,[1] and the dynamics of a flow or a map can be modeled as a probabilistic dynamical system. In this study we take a somewhat different point of view. We are interested in the interplay between the geometrical objects in the flow, like lobes[2] and KAM tori and the statistics of the passive scalar motion. A commonly observed property of fluid flows at the time-scales at which molecular diffusion is not important is nonhomogeneity of passive scalar distributions. The phenomena in which we are interested are finite-time phenomena. This makes sense given the spatial extent of problems that we study: Cellular flows and motion in the Gulf Stream modeled as a meandering jet. Besides being topics of research of many research teams, these problems are paradigms of two situations, the difference of which we want to emphasize: Cellular flows that we study have zero (temporal) mean velocity, while jets have nonzero mean velocity.

The concept that we use most in this study is the Lagrangian velocity average, i.e. the average of the velocity field along fluid particle trajectories. We introduce the second moment of the distribution of Lagrangian velocity averages as a measure of patchiness of the flow. This is suggested by the dispersion behavior of nonhomogeneous flows. The initial dispersion behavior of such flows is quadratic in time [Mezić, 1994]. If nonhomogeneity of Lagrangian time-averages is preserved at longer times, i.e. if the Lagrangian time-average of velocity is not constant for almost every initial condition, the quadratic dispersion in time persists. As shown in detail below, it is then interesting to monitor the development in time of patchiness — the second moment of the distribution of Lagrangian velocity. We will show that this quantity decays to zero if the flow is ergodic or if the velocity field has a zero time average. In fact, it provides a good indicator of the mixing behavior of the flow. If patchiness tends to a constant different from zero, the flow is not ergodic. If the flow is ergodic, then patchiness decays to zero. The scaling of patchiness as time goes to infinity is associated with the scaling of dispersion.

We also suggest that density plots of Lagrangian velocity averages are useful tools for the study of finite-time mixing and transport in fluid flows. In these plots, the color is associated with

[1]We define the notion of "mixing" for a dynamical system. Let M be a space equipped with a measure denoted by μ. Let ϕ_t be a one-parameter family of automorphisms of M that depends measurably on t. Then ϕ_t is said to be mixing if $\lim_{t\to\infty} \mu(\phi_t(A) \cap B) = \mu(A)\mu(B)$, for every pair of measurable sets $A, B \subset M$. For more details see [Arnold & Avez, 1968]. Mixing implies ergodicity, but ergodicity does not imply mixing.

[2]A *lobe* is a region bounded by segments of stable and unstable manifolds of a hyperbolic trajectory, or the stable and unstable manifolds of two different hyperbolic trajectories. Lobes are important because they are invariant regions that transport fluid, see [Wiggins, 1992].

velocity averages. These plots are patchy — the predominant feature in them are blobs of the same color. This indicates lack of mixing in these regions, as sampling different velocities is related with exploration of the phase-space. The patchiness plots have features closely related to the geometrical objects in the flow — invariant regions around elliptic fixed points and lobes. For example, in an invariant elliptic region in the flow, time averages of the velocity converge very quickly to a constant value (which can be nonzero or zero, depending on whether that elliptic region is an accelerator mode or not (see [Mezić & Wiggins, 1995b]). Lobes transfer particles from one zone in the physical space to another [Wiggins, 1992] and contribute to mixing. Particles in a lobe lose uniformity of velocity averages by intersecting with other lobes.

Patchiness plots give color-coded indication of the nature of the dynamics, and although we test the newly introduced concepts on two-dimensional flows, they might prove to be particularly important in three-dimensional flows where Poincaré maps are not as revealing as in the two-dimensional case.

1.1. *Patchiness in fluid flows*

The patchiness in fluid flows is characterized by the presence of a huge number of small localized regions (i.e. patches) that have average velocity significantly different than the area surrounding them. The existence of patchiness implies a strong dependence of the dispersion behavior on initial location in space. Pasmanter [1988, 1991], while studying the variability of dispersion processes in the ocean, observed that the dispersion of the fluid particles in laminar incompressible flows exhibit the phenomenon of patchiness. He also found that the presence of patchiness led to anomalous diffusion behavior of the passive tracers. In this paper we examine the nature of the patches in detail and interpret the transport properties of the passive particle trajectories in terms of underlying patchiness behavior.

1.2. *Lagrangian transport of passive tracers*

Consider a general incompressible velocity field in two-dimensional space (x, z)

$$\dot{x} = v_x(x, z, t) = -\frac{\partial \psi}{\partial z}(x, z, t)\,,$$

$$\dot{z} = v_z(x, z, t) = \frac{\partial \psi}{\partial x}(x, z, t)\,, \tag{2}$$

For a fluid particle initially located at $(x(0), y(0))$, the horizontal transport can be characterized in terms of the finite time average along particle trajectories of the x-component[3] of the velocity field, and is given as follows.

$$\overline{v}_x(t) = \frac{1}{t}\int_0^t v_x(x(\tau), z(\tau), \tau)d\tau$$

$$= \frac{x(t) - x(0)}{t}\,. \tag{3}$$

Thus, the x-component of the trajectory $(x(t), z(t))$ can be expressed as

$$x(t) = x(0) + \overline{v}_x(t)t\,. \tag{4}$$

The velocity field is defined over a two-dimensional domain A, and let $p(x, z)$ be the initial distribution of some ensemble of initial conditions over the domain A. At time t, the mean displacement and the dispersion are defined as

$$m_x(t) = \langle x(t) - x(0)\rangle = \int_A [x(t) - x(0)]p\,d\mu\,, \tag{5}$$

and,

$$D_x(t) = \langle [x(t) - x(0) - \langle x(t) - x(0)\rangle]^2\rangle$$

$$= \int_A [x(t) - x(0) - \langle x(t) - x(0)\rangle]^2 p\,d\mu\,, \tag{6}$$

where $d\mu$ $(= dx\,dz)$ represents the measure of some area element on A. Using (4)–(6), it is easy to see that

$$m_x(t) = m_v(t)t\,, \tag{7}$$

and

$$D_x(t) = D_v(t)t^2 \tag{8}$$

where

$$m_v(t) = \langle \overline{v}_x(t)\rangle\,, \tag{9}$$

$$D_v(t) = \langle [\overline{v}_x(t) - m_v(t)]^2\rangle\,. \tag{10}$$

[3]The dependence of average velocity component on its initial condition is assumed to be implicit, and is not shown in the argument(s).

Here, $D_v(t)$ represents the dispersion of patchiness behavior as a function of time, and it monitors the progress of the spatial inhomogeneities in the velocity field that a particle observes. In the finite time, the behavior of $D_v(t)$ effectively determines the resulting dispersion behavior of the tracer particles in the time-dependent velocity fields.

The conditions for the asymptotic behavior of the dispersion are formally obtained in [Mezić & Wiggins, 1994]. They used Birkhoff's Ergodic Theorem to obtain necessary and sufficient conditions for the existence of anomalous (t^2) dispersion behavior in nondiffusive passive particles in a class of incompressible laminar flows. They show the nonergodicity to be the dynamical mechanism giving rise to such dispersion behavior (see [Mezić, 1994; Mezić & Wiggins, 1994]).

The limiting value of $D_v(t)$ as $t \to \infty$, which exists if the velocity is bounded, is equal to

$$a = \langle [\overline{v}_x^* - \langle \overline{v}_x^* \rangle]^2 \rangle$$

where

$$\overline{v}_x^* = \lim_{t\to\infty} \overline{v}_x(t) = \lim_{t\to\infty} \frac{1}{t} \int_0^t v_x(x(\tau),\, z(\tau),\, \tau) d\tau$$

is the infinite-time average of the horizontal velocity. From (8) it is clear that t^2 dispersion is possible only when $D_v(t)$ approaches a constant limiting value different from zero, thus providing a sufficient condition for the t^2 dispersion behavior in the advection of two-dimensional velocity fields. The relation of this result to lack of ergodicity can be seen as follows. If Birkhoff's ergodic theorem (or some other appropriate ergodic theorem) is applicable then $\langle \overline{v}_x^* \rangle = \langle \overline{v}_x \rangle$. In this case we have $a = \langle [\overline{v}_x^* - \langle \overline{v}_x \rangle]^2 \rangle$, and $a = 0$ implies $\overline{v}_x^* = \langle \overline{v}_x \rangle$, or the time average of v_x equals the space average of v_x, which is true if the flow is ergodic. Hence, if $D_v(t)$ goes to a constant different from zero when time goes to infinity, the velocity field is not ergodic and different initial conditions can have different Lagrangian time-averages of velocity. We also see that $a = 0$ in the case where the flow has temporal mean zero. In this case the flow can be nonergodic, yet $D_x(t)$ does not behave asymptotically like t^2.

1.3. *Statistical and geometric features of Lagrangian trajectories*

In the study of fluid mixing, mean square displacement $D(t)$ at time t of the passive tracers (hence the flow trajectories) is an important measure of dispersion of the fluid particles. In the presence of molecular diffusion it is well known that the mean square displacement varies linearly with time, and such behavior is referred to as *diffusive*. When the variance of the tracer particles grows nonlinearly with time, the dispersion behavior is referred to as *anomalous diffusion*. As seen earlier [refer to Eq. (10)], the dispersion of particle trajectories in any velocity-field is determined by the dispersion of patchiness.

The nature and stability of the probability distribution of the patches also yields crucial information about the particle transport. The origin and spatial location of these patches is also of interest to us. These are intimately related with the basic geometric structures (such as stable and unstable manifolds and their intersections) associated with the flow.

1.4. *Two case studies*

We consider two different kinematic flow fields[4] First, we examine the patchiness behavior associated with the a model of a Rayleigh–Bénard flow used to study cell-to-cell transport in the presence of the even-oscillatory instability (see [Camassa & Wiggins, 1991]). The mean velocity is zero for this flow. Next, a model of a meandering jet[5] (originally due to Bower [1991]) is considered, where we study the effect of periodic and quasi-periodic meridional flow on such a jet. The jet travels with a nonzero mean velocity.

In addition, we also investigate the effect of white noise on the patchiness structure in both the cases. It should be mentioned that the techniques developed here are not limited to the availability of kinematic models, but can be easily modified to accommodate numerically generated velocity fields from the dynamically consistent models.

[4]By the term "kinematic model" we mean a vector field whose trajectories and phase space structures, i.e. kinematic features, model similar features that are observed in certain types of fluid flows. Thus, kinematic models are not solutions of the fluid mechanical equations of motions.

[5]A "jet" is described by a velocity field containing a localized region in which the velocity in a certain direction is much larger than the velocity in the same direction for the surrounding fluid. The jet is said to be a "meandering jet" if its spatial stucture varies in space. In our example such a variation will be sinusoidal.

2. Lagrangian Transport in Cellular Flows

In this section we consider the classical Rayleigh–Bénard convection in two dimensions. We consider a steady convection cell whose horizontal length is much larger than its height, and the convection cells are aligned along the y-axis. For this flow, an explicit form of the velocity field was obtained by Chandrasekhar [1961] under the assumptions of stress-free boundary conditions and single mode convection. The stream function is given as

$$\psi_0(x,\, z) = \frac{A}{k} \sin(kx) \sin(\pi z)\,, \tag{11}$$

and the associated velocity field is given by

$$\begin{aligned} \dot{x} &= -\frac{\partial \psi_0}{\partial z}(x,\, z) = -\frac{A\pi}{k} \sin(kx) \cos(\pi z)\,, \\ \dot{z} &= \frac{\partial \psi_0}{\partial x}(x,\, z) = A\, \cos(kx) \sin(\pi z)\,, \end{aligned} \tag{12}$$

where A is the maximum vertical velocity, and $k = 2\pi/\lambda$ is the wave number in the horizontal direction. The length measures are nondimensionalized such that the top and the bottom of the cells are at $z = 1$ and $z = 0$, respectively. The streamlines for the steady flow are shown in Fig. 1 for $A = 1$, and $k = 2$. In this case, the steady flow is confined in two-dimensional spatially periodic cells, with period π in the x-direction, and lies between the boundaries at $z = 0$ and $z = 1$. The steady velocity field has two types of hyperbolic fixed points located at $(j\pi/k,\, 0)$ and $(j\pi/k,\, 1)$, respectively, for $j = 0, \pm 1, \pm 2, \ldots$. The fixed points that have the same x coordinate on the upper and the lower wall are connected by a vertical boundary (a heteroclinic connection).

For two adjacent cells, the interior flow consists of closed circulatory motion moving clockwise for one cell and counterclockwise for another, and the pattern repeats itself after each λ distance resulting in a stream of infinite cells, or rolls (Note: In the context of this problem, throughout the literature the terms "rolls" and "cells" are used synonymously). For this flow our concern lies in the transport of a passive tracer from cell-to-cell. For the steady velocity field, the flow inside each cell is distinctly separated by a dividing stream line (i.e. the heteroclinic orbit). Each of these vertical heteroclinic connections separates clockwise flow from the counterclockwise flow, and in the absence of molecular diffusion these barriers act to completely inhibit any transport between the cells.

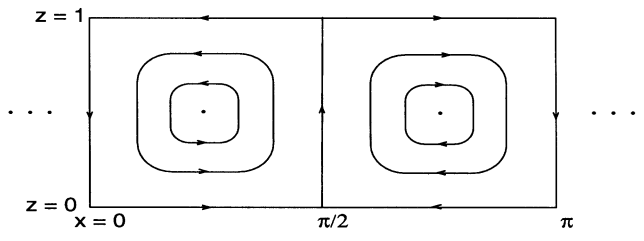

Fig. 1. Steady flow in the row of convection cells.

2.1. *Effect of periodic disturbances*

If the temperature difference between the top and the bottom walls is increased, a time-periodic instability occurs which results in time-periodic velocity field. In the presence of time-periodicity (no matter how small), the dividing streamlines break and allow inter-cell transport and chaotic fluid particle trajectories. Based on their experimental results of roll-to-roll transport of a passive tracer, Solomon and Gollub [1988] introduced the following unsteady stream function,

$$\begin{aligned} \psi(x,\, z,\, t) = \frac{A}{k} \sin(\pi z)[&\sin(kx) \\ &+ \varepsilon k\, \cos(kx) \cos(\omega t)]\,, \end{aligned} \tag{13}$$

The time-dependence corresponds to the collective oscillation of the roll boundaries in the perpendicular direction of the roll-axes. This phenomenon is known as the even oscillatory instability. The corresponding time-dependent velocity field is given as

$$\begin{aligned} \dot{x} &= -\frac{\partial \psi}{\partial z}(x,\, z,\, t) \\ &= -\frac{A\pi}{k} \cos(\pi z)[\sin(kx) + \varepsilon k\, \cos(kx) \cos(\omega t)]\,, \\ \dot{z} &= \frac{\partial \psi}{\partial x}(x,\, z,\, t) \\ &= A\, \sin(\pi z)[\cos(kx) - \varepsilon k\, \sin(kx) \cos(\omega t)]\,, \end{aligned} \tag{14}$$

where $\omega = 2\pi/T$ is the frequency associated with the time-dependent instability, T is the corresponding period, and ε is proportional to the square-root of the difference between the Rayleigh number from its critical value corresponding to the onset of the even oscillatory instability. For a detailed description of the mechanism for roll-to-roll fluid transport, the reader is referred to [Camassa & Wiggins,

1991]. In this flow, we are interested in obtaining a quantitative measure of the fluid moving in and out of the cell boundaries, and the qualitative nature of the fluid particle trajectories that participate in cell-to-cell transport. We are also interested in locating the subdomains within a cell that are likely to disperse at the most efficient rate, and in relating these to the geometric structures in the flow, such as invariant manifolds. Since the top and the bottom boundaries of the cells are rigid, the transport primarily occurs in the horizontal direction. We next present the results from some numerical experiments showing the dispersion behavior in the Rayleigh–Bénard flow.

2.2. *Description of the patchiness structure*

In time-periodic cellular flow the time average of the x-component of velocity along the Lagrangian trajectories $(x(t), z(t))$ is given by

$$\overline{v}_x(t) = -\frac{1}{t}\int_0^t \frac{A\pi}{k}\cos(\pi z(\tau))[\sin(kx(\tau)) + \varepsilon k\cos(kx(\tau))\cos(\omega\tau)]d\tau \qquad (15)$$

This can be computed numerically over an appropriate domain. It is sufficient to consider a domain covering a single cell. For illustrative purposes, we consider a domain consisting of two adjacent cells ($x \in [0, \pi]$, $z \in [0, 1]$). This domain consists of a uniform grid of 300×100 grid points. We plot the average x-velocity contours on the initial grid. The same color in any picture corresponds to a subdomain with the same average x-velocity.

- The first slice in Fig. 2 shows the initial configuration of the x-velocity (at time $t = 0$), and the remaining slices give the average x-velocity contours at the respective times. In subsequent pictures at $t = T, 2T, 3T, \ldots$, we observe the deformation of the initial contour configuration.
- In the beginning, the contour structure deforms along the unstable manifolds and gives a reasonably good template for the unstable manifolds of the three hyperbolic (periodic) orbits in the domain and the KAM tori in a relatively short time of integration (within $3T$). For comparison, the reader is referred to Fig. 29 for the associated manifold geometry.
- This contour structure starts to disintegrate into big patches, and these big patches further dissociate into smaller and smaller structures. The patches represent regions of relatively much larger *magnitude* of the average x-velocity than the region surrounding them. These patches are primary regions for the intercellular transport.
- These patches persist for as long as the numerical trajectories are computed, although their relative strength (i.e. the magnitude of the associated average-velocity) diminishes.
- The qualitative nature of the patchiness behavior remains the same when we change the amplitude (ε) or the associated frequency (ω) of the oscillatory instability.

In time-dependent nonlinear flows, the individual particle trajectories may be unstable for small perturbations, however the statistical properties of the tracer trajectories are robust and reproducible. Thus, the statistical properties of the patches are important for understanding the mixing behavior in the flow. The distribution of the patchy structures, and the dispersion behavior of the passive tracers is discussed next.

2.2.1. *Distribution of patchiness*

The distribution of the average x-components of velocity for particle trajectories is shown at four different time intervals in the following diagrams. The bin-width is chosen to be 0.005 for time-periods less than 10, and 0.002 for all other times. The following features are noted:

- The mean flow is zero in the x-direction for the cellular transport case. This means the net flow through the left boundary of the cell is the same as the net flow through the right boundary.
- The probability distributions are always symmetric about the zero mean flow in the x-direction, implying that the left moving and the right moving patches are evenly distributed in the cell domain.
- The probability distribution approaches the appearance of a normal distribution very fast when the amplitude of the time-dependence is high, i.e. large values of ε (see Figs. 4 and 5).
- For lower values of ε (say, $\varepsilon = 0.1$), the distribution takes an extremely long time to settle to normal distribution. In this case, the probability distribution remains non-Gaussian even after 100 periods (see Fig. 3).
- None of the distributions reach an equilibrium even after 1000 time-periods.

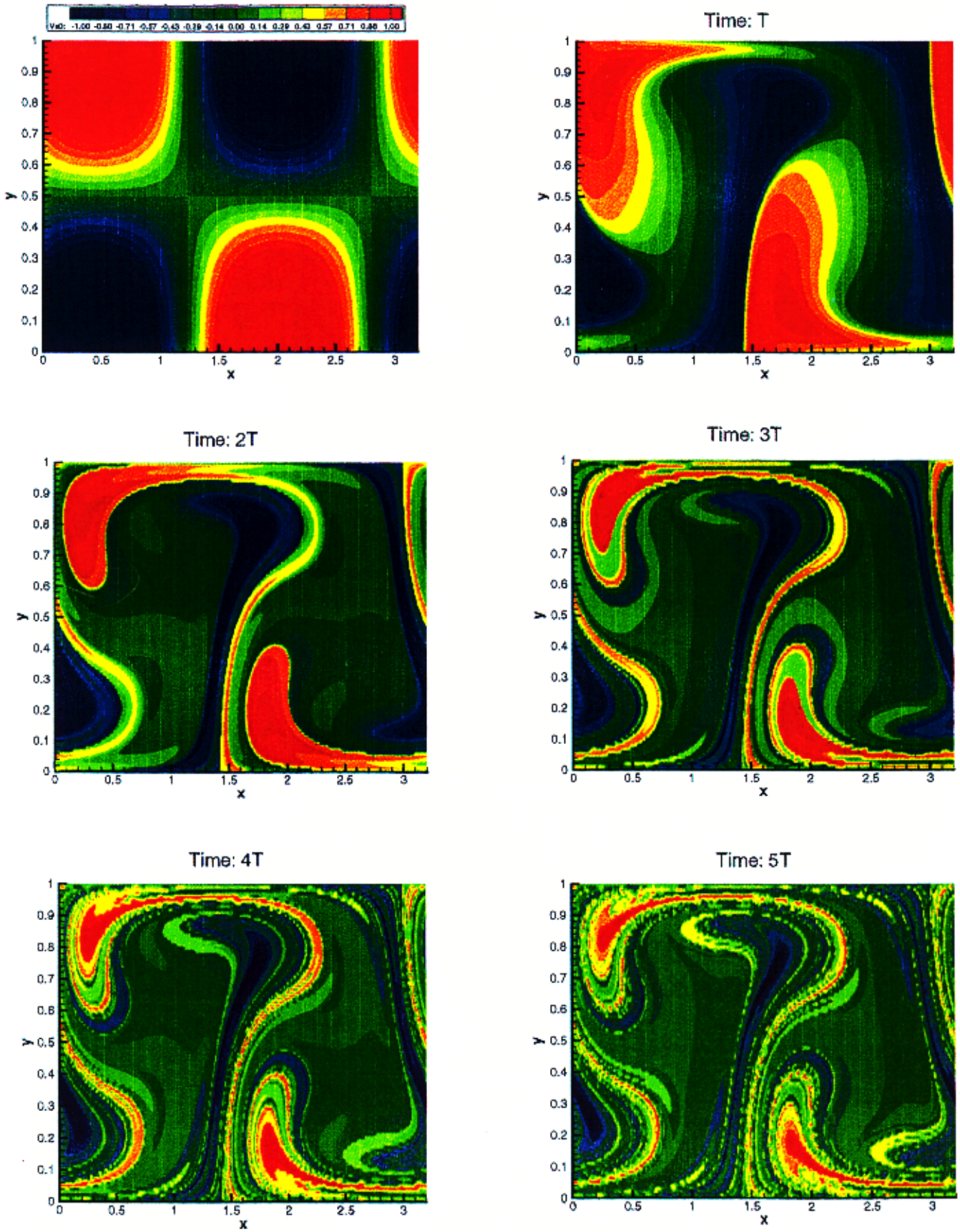

Fig. 2. Average x-velocity contours corresponding to initial points having the same time-average along the tracer trajectories. The parameters are fixed at $A = 1$, $k = 2$, $\omega = 4.2$, and $\varepsilon = 0.1$.

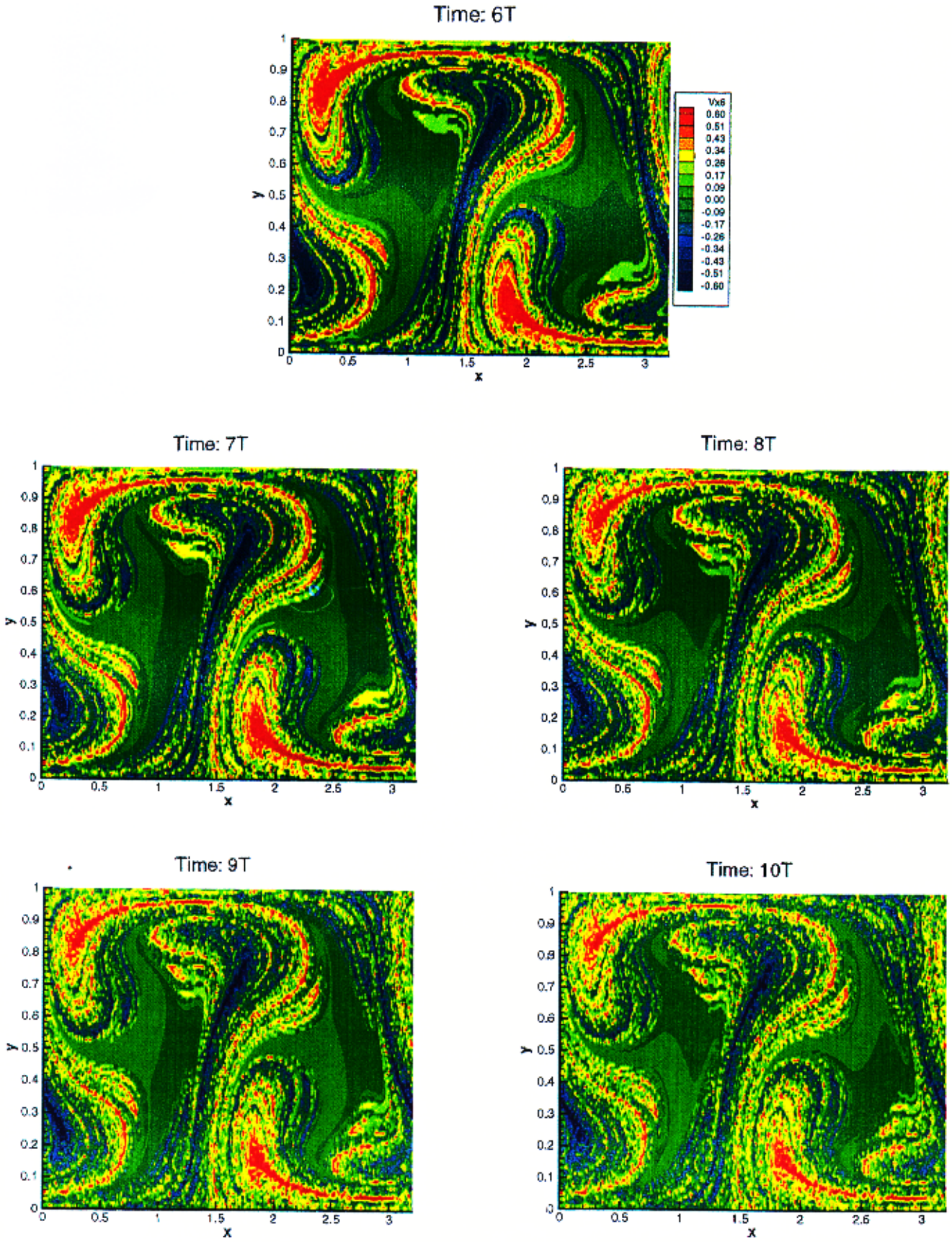

Fig. 2. (*Continued*)

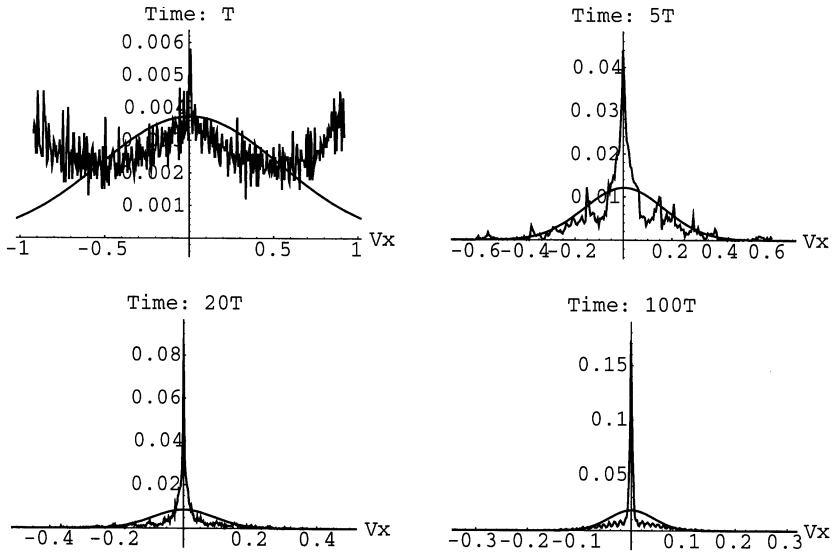

Fig. 3. The probability distribution of the averaged x-component of velocity at time T, $5T$, $20T$, and $100T$. Other parameters are set at $A = 1$, $k = 2$, $\omega = 4.2$, and $\varepsilon = 0.1$. On the vertical axis, the fraction of total points is plotted.

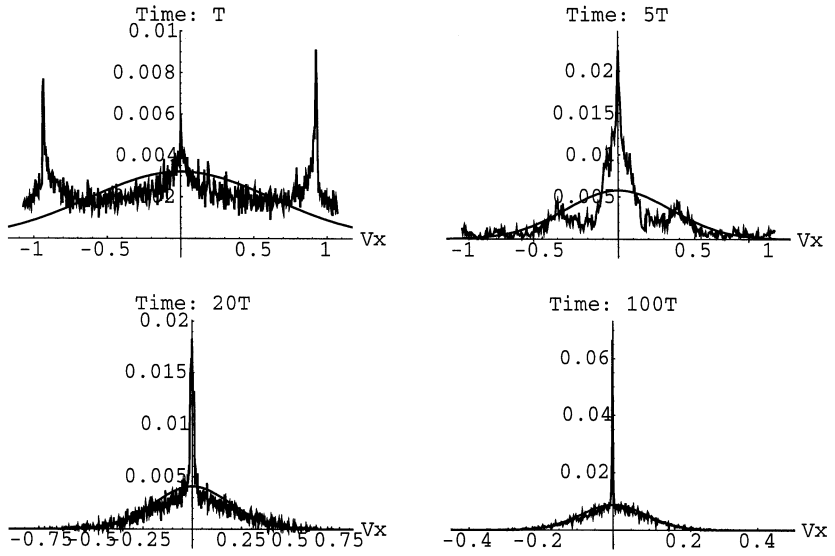

Fig. 4. Same as Fig. 3 except $\varepsilon = 0.4$.

2.2.2. *Dispersion characteristics*

The resulting dispersion of the tracer particles depends on the dispersion of the patches [from Eq. (8)]. In fact, the dispersion of the particle trajectories is directly proportional to the dispersion of patchiness. Figure 6 shows the dispersion behavior of the patches, and Fig. 7 shows the corresponding dispersion law ($D_x(t)$) for the passive tracers for three values of ε, the strength of the time-dependence of the velocity field. Figure 8 shows similar characteristics for two different values of the frequency ω. We note the following features.

- $D_v(t)$ is found to be proportional to $t^{-\gamma}$, where γ is referred to as the *patchiness exponent*. Thus, $D_x(t)$ increases like t^{γ_x}, where $\gamma_x = (2 - \gamma)$.
- In all the cases examined, the value of the exponent γ_x lies between 1.06 and 1.08 for up-to 100 time-periods. The scaling law for the particle trajectories between 100 and 1000 periods gives the exponent γ_x to be approximately 1.02 (see Figs. 9 and 10). The patchiness exponent approaches 1

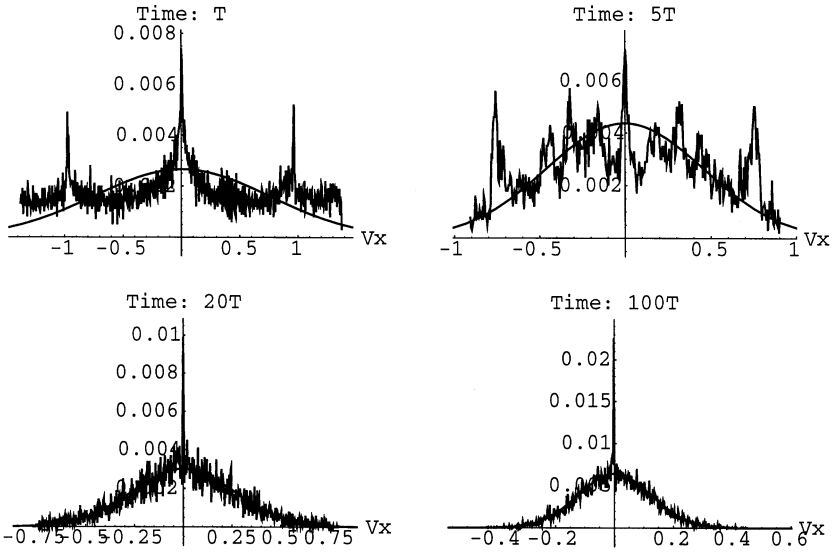

Fig. 5. Same as Fig. 3 except $\varepsilon = 0.8$.

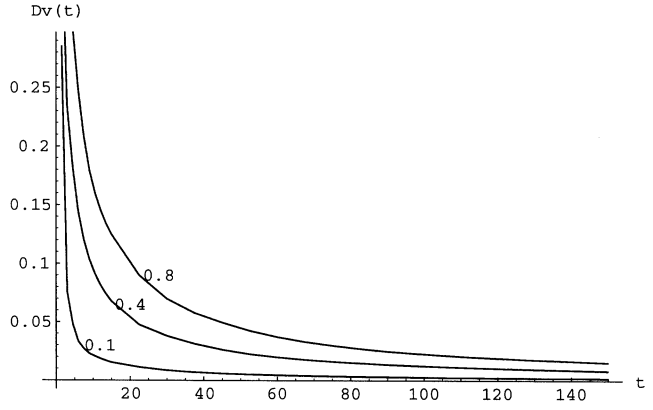

Fig. 6. Dispersion of patches of average x-velocity as function of time, for three different ε values.

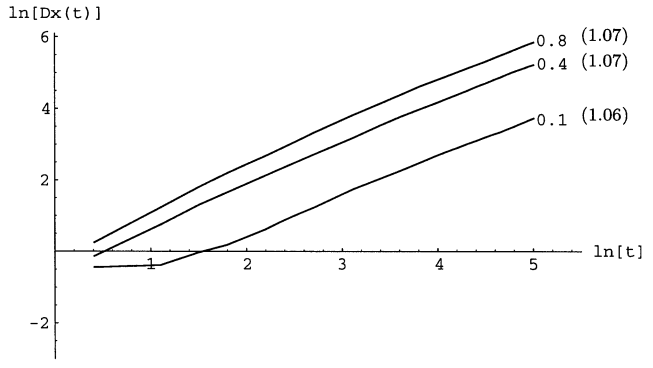

Fig. 7. Dispersion law for the passive tracers corresponding to Fig. 6. The associated values of the slope (or exponent γ_x) is shown in the parenthesis.

as $t \to \infty$, thus implying a linear dispersion law in the asymptotic limit.

- Solomon and Gollub [1988] experimentally observed that the effective diffusion constant grows linearly with the amplitude of time-dependence. A simple Melnikov type calculation also shows the effective diffusion constant is directly proportional to ε (see e.g. [Chirikov, 1979]). Our numerical results confirm the linear dependence of advective diffusion constant on the amplitude of the lateral oscillation. Figure 11 shows the evolution of the ratio $R(\varepsilon_1, \varepsilon_2, t)$ for three different combinations of amplitude values, where

$$R(\varepsilon_1, \varepsilon_2, t) = \frac{D_v(t)|_{\varepsilon_1}}{D_v(t)|_{\varepsilon_2}}, \tag{16}$$

In all three cases the ratio $R(\varepsilon_1, \varepsilon_2, t)$ settles to a value very close to $\varepsilon_1/\varepsilon_2$ very fast. This shows the robustness of the linear dependence of the dispersion behavior on the amplitude.

2.3. *Discussion*

The characteristics of the probability distribution function of the patchiness explain the observed dispersion behavior in the cellular transport case. The long-term dispersion law $D_x(t)$ is proportional to t because the dispersion of patchiness $D_v(t)$ decays

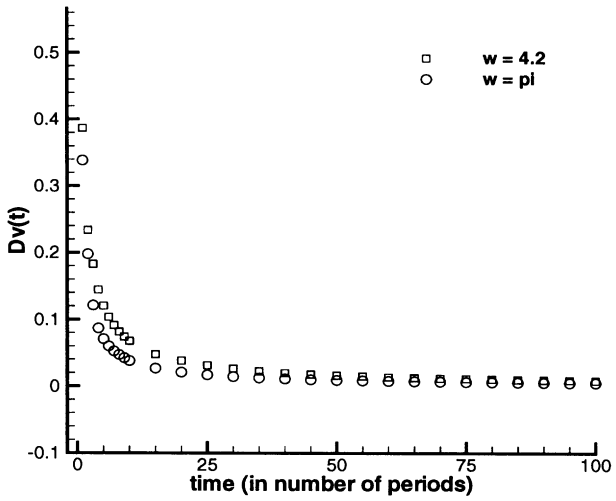

(a)

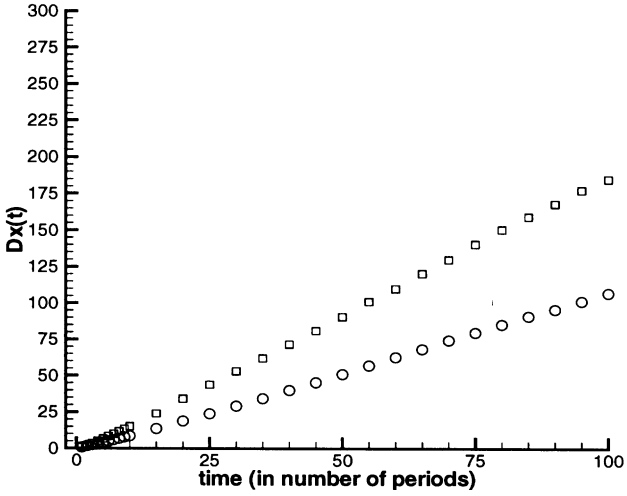

(b)

Fig. 8. (a) Dispersion of patches of average x-velocity, and (b) Dispersion law for the passive tracers, for two different frequencies.

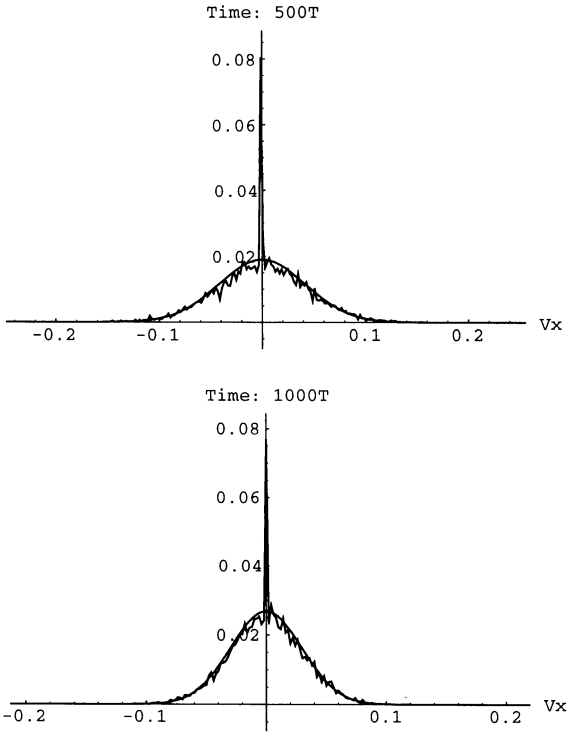

Fig. 9. Same as Fig. 3 except $\varepsilon = 0.4$.

like $1/t$. The dispersion of patchiness decays because the symmetric probability distribution continuously shrinks towards the zero mean flow in the cell-flow case. This further implies that the patches diminish in strength as $t \to \infty$, and thus the rate at which the trajectories (initially contained in cell R_0) invade the cells (on the right or the left) slows down continuously as $t \to \infty$. This is precisely what we observe when we examine the spreading of the passive tracers which are initially contained in cell R_0. We show the distribution of passive particles among various cells as a function of time in Fig. 12 for $\varepsilon = 0.1$, 0.4 and 0.8, respectively. Here, the color scheme is chosen such that various colors correspond to different cells or cell-clusters. In this figure, one can spot at various times the current cell R_j of all passive scalars that were initially located in the reference cell R_0.

The ratio of trajectories, $F_e(t)$, that escape the reference cell R_0 through the left or right boundary is shown in Fig. 13 as a function of time for up to 1000 time-periods for all three cases. For relatively high values of amplitude of time-dependence, most trajectories escape the reference cell R_0 within the first 15 to 20 periods, and beyond that $F_e(t)$ approaches a steady limit. This is expected since $(1 - F_e(\infty))$ gives the area within the KAM tori on the time-slice. On the other hand, for small values of ε more and more trajectories continue to escape from R_0 and as a result $F_e(t)$ steadily grows even beyond 1000 periods.

3. Lagrangian Transport in a Meandering Jet

We next consider Lagrangian transport in meandering jets. We examine the motion of fluid particle trajectories in the two-dimensional kinematic model of a meandering jet originally proposed by Bower [1991]. This model, based on RAFOS float observations, consists of a jet of uniform width which

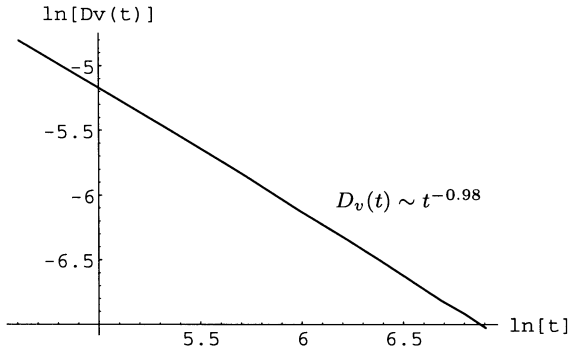

(a)

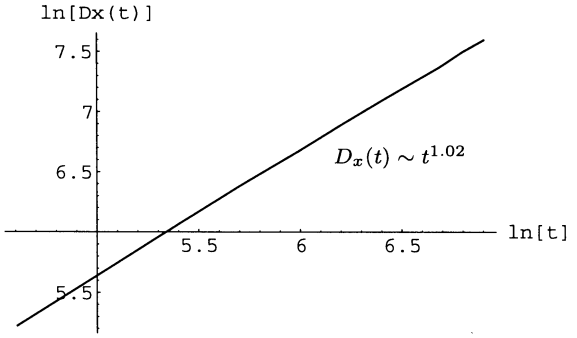

(b)

Fig. 10. The dispersion of (a) patchiness, and (b) particle trajectories, between $100T$ and $1000T$.

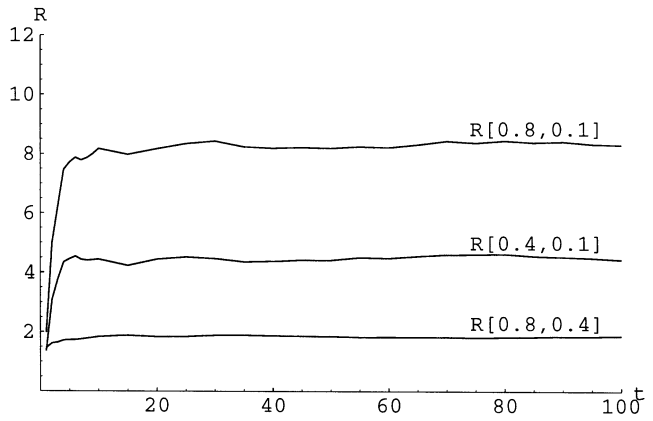

Fig. 11. The ratio of $D_v(t)$ for different values of ε versus time.

is deformed by a steadily propagating sinusoidal meander. This jet, when examined in a reference frame moving with the meander, has three distinct regimes of fluid flow, a central jet, exterior retrograde motion, and intermediate closed circulations above meander troughs and below meander crests. In this model, no transport is possible between the three regimes because the flow is steady. In order to make the fluid exchange possible among the regimes, Samelson [1992] introduced spatiotemporal variability in the regular velocity field of Bower. He considered three different kinds of time-periodic irregularities in the steady velocity field, and using Melnikov's method and numerical computations he provided a quantitative measure of transport between different regions of the meandering jet. Samelson's model was reconsidered by Duan and Wiggins [1996] by taking quasi-periodic spatiotemporal variability in the velocity field to provide detailed computations of finite and infinite-time fluxes between the different regimes of the flow as a function of various perturbation parameters such as amplitude and frequency of the time-dependence in the moving reference frame. Here, we revisit the model considered by Duan and Wiggins [1996] to examine the geometric and statistical properties of the passive particle trajectories in a reference domain that is spatially periodic in the horizontal direction.

The stream-function for the meandering jet in a stationary frame of reference is given as (see [Bower, 1991; Samelson, 1992]):

$$\psi(X, Y, t) = \psi_0 \left[1 - \tanh\left(\frac{Y - A\cos k(X - c_x t)}{\lambda[1 + k^2 A^2 \sin^2 k(X - c_x t)]^{\frac{1}{2}}}\right)\right] \tag{17}$$

where X and Y are the eastward and northward Cartesian coordinates, respectively, $2\psi_0$ represents the net eastward transport, A, c_x, and k are the amplitude, phase-speed, and the wavenumber of the meander, and the parameter λ determines the width of the jet. In a reference frame moving with the meander, the coordinates are given as follows after scaling them with λ.

$$x = \lambda^{-1}(X - c_x t)\,, \quad y = \lambda^{-1} Y\,. \tag{18}$$

In this reference frame the stream function takes the following form

$$\phi(x, y, t) = 1 - \tanh\left(\frac{y - B\cos \kappa x}{[1 + \kappa^2 B^2 \sin^2 \kappa x]^{\frac{1}{2}}}\right) + cy \tag{19}$$

where

$$\phi = \psi_0^{-1}\psi + cy\,, \quad B = \lambda^{-1} A\,,$$
$$\kappa = 2\pi L^{-1} = k\lambda\,, \quad c = \lambda\psi_0^{-1} c_x\,,$$

and the nondimensional time is given by $\tau = \psi_0 \lambda^{-2} t$. The associated velocity field in the frame

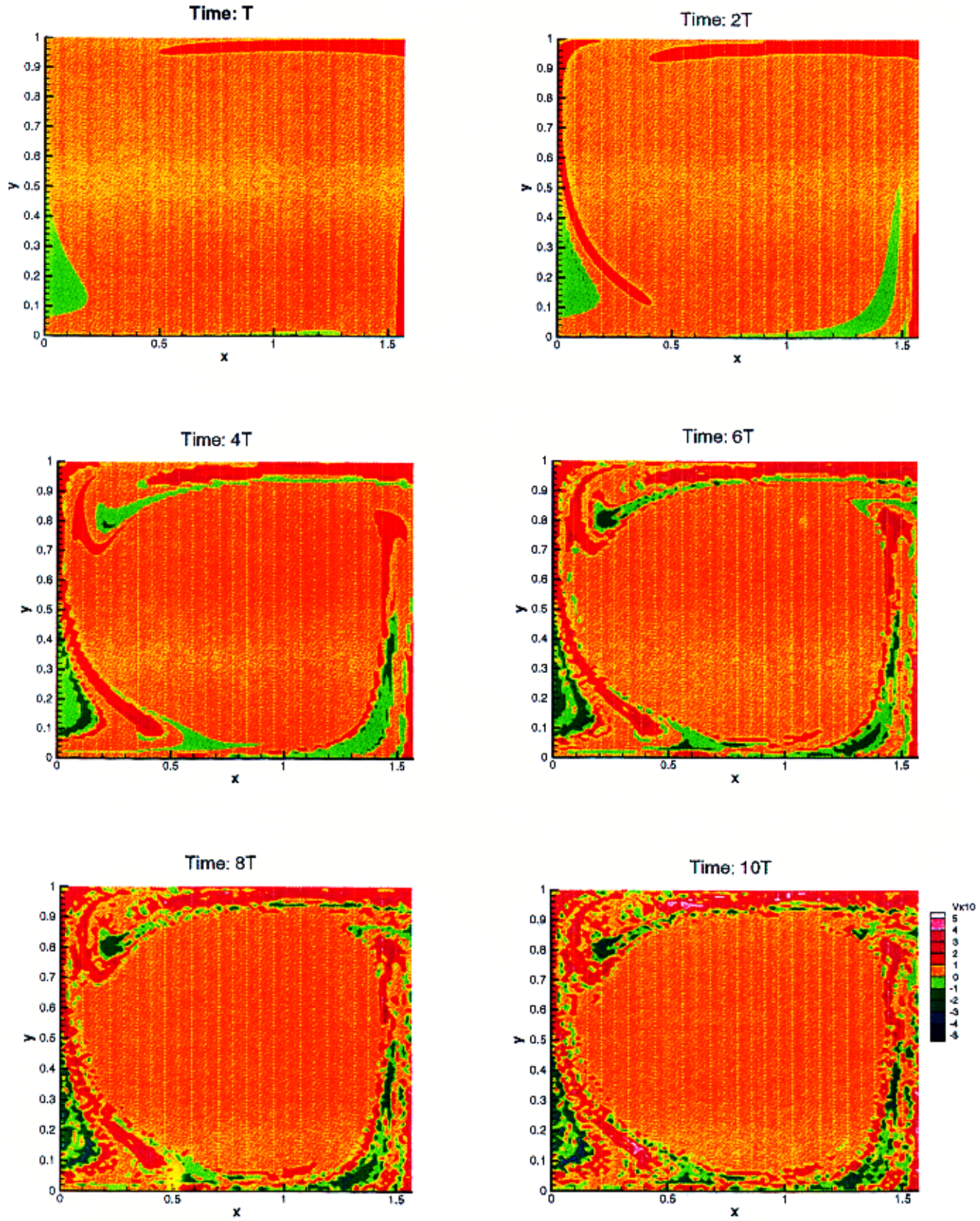

Fig. 12. The distribution of initial points colored according to which cell they invade as a function of time, for $\varepsilon = 0.1$, 0.4 and 0.8, respectively. The other parameters remain identical to Fig. 2. Initially all the passive tracers are located in cell R_0, and subsequently escape to the other cells. The color scheme is chosen such that various colors correspond to different cells or cell-clusters.

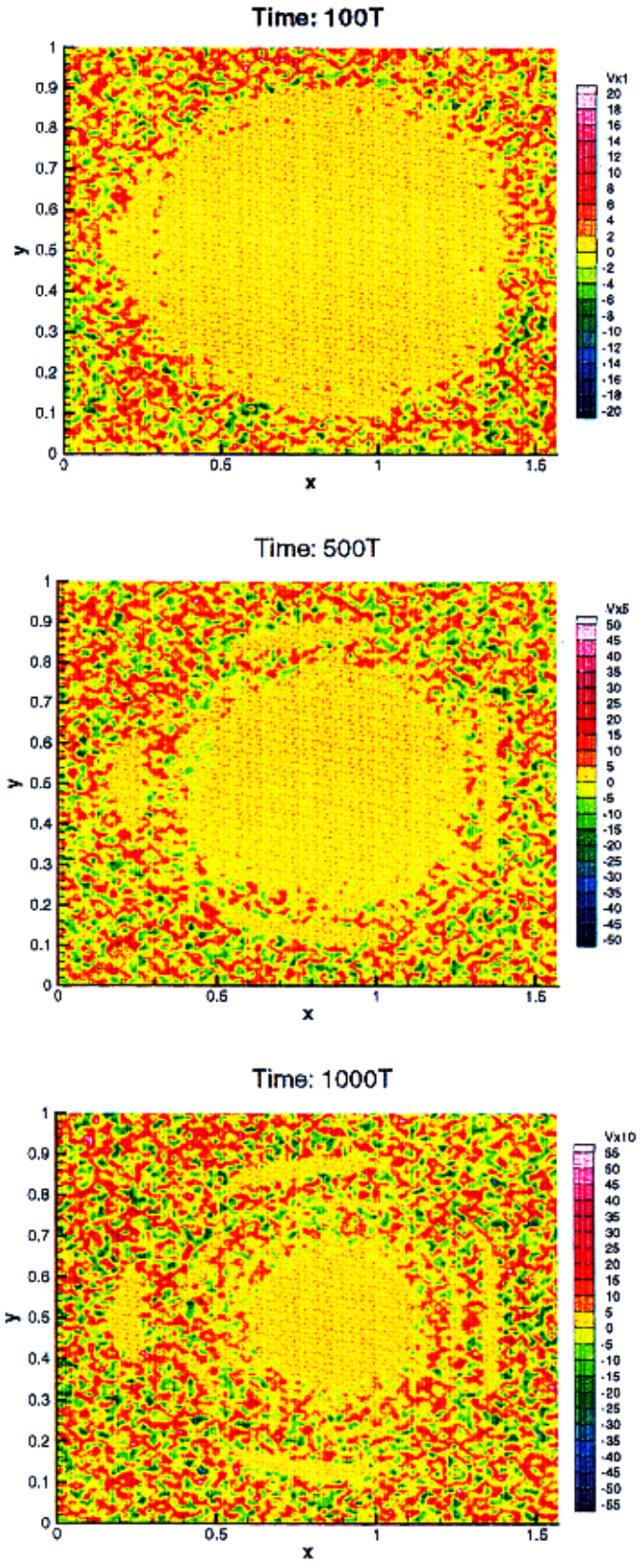

Fig. 12. (*Continued*)

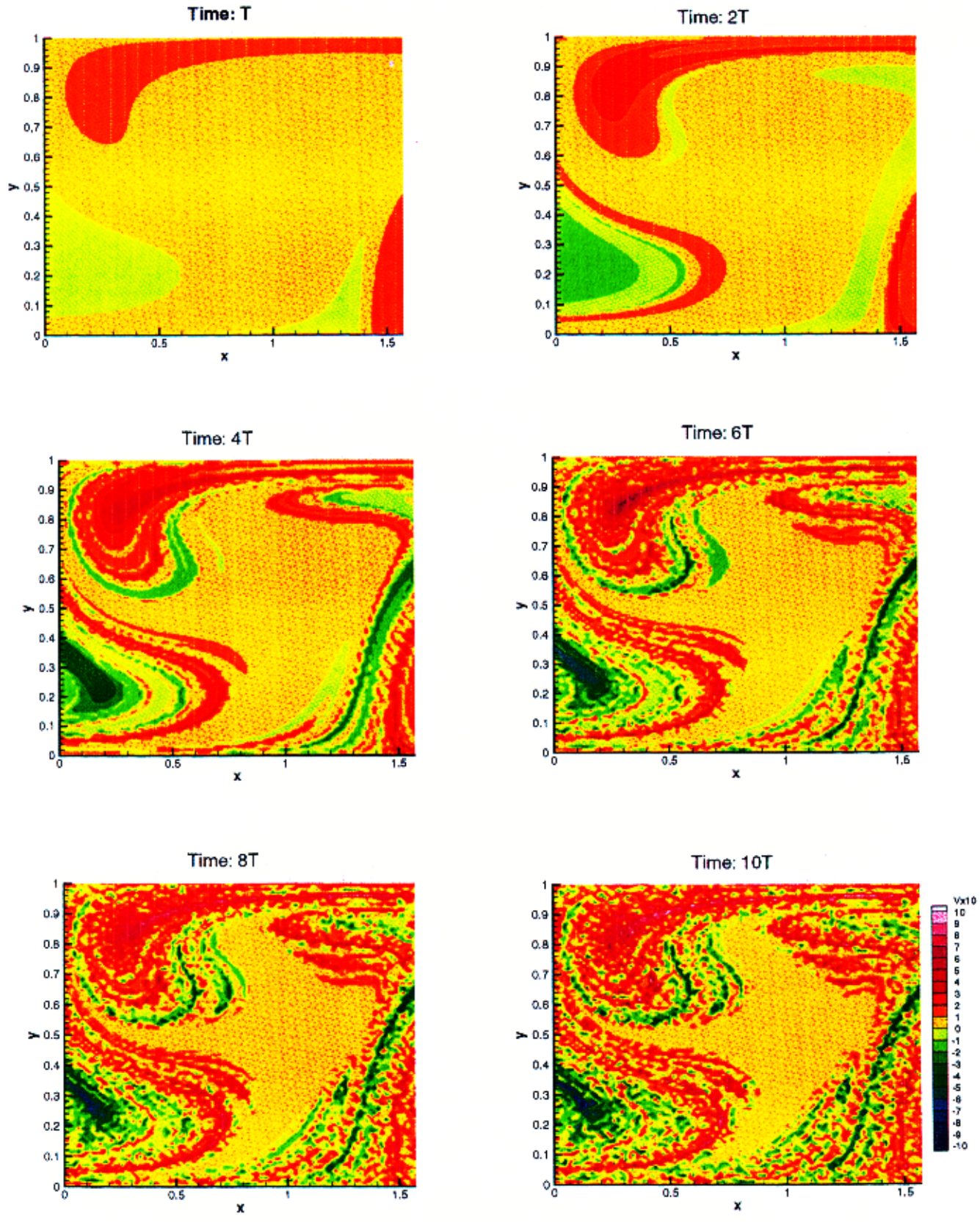

Fig. 12. (*Continued*)

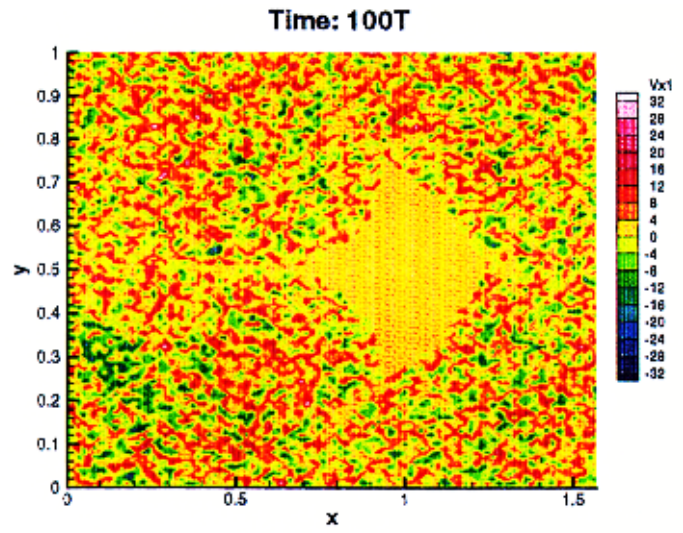

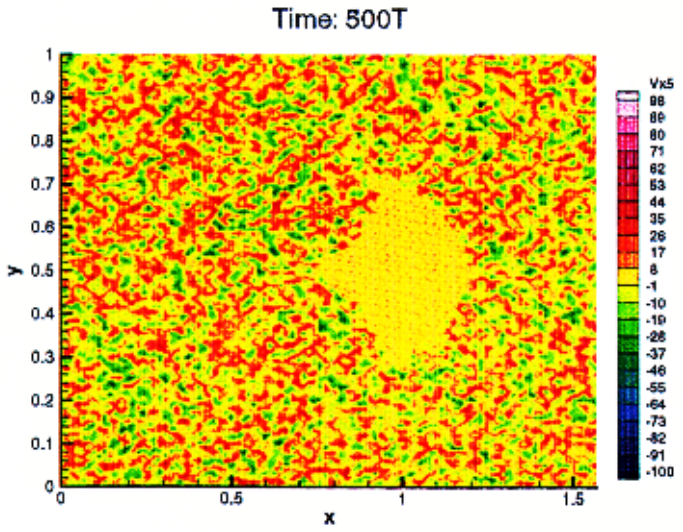

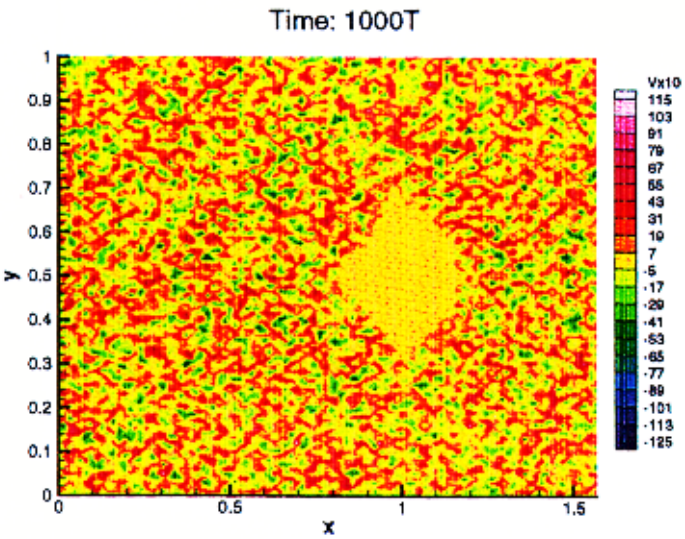

Fig. 12. (*Continued*)

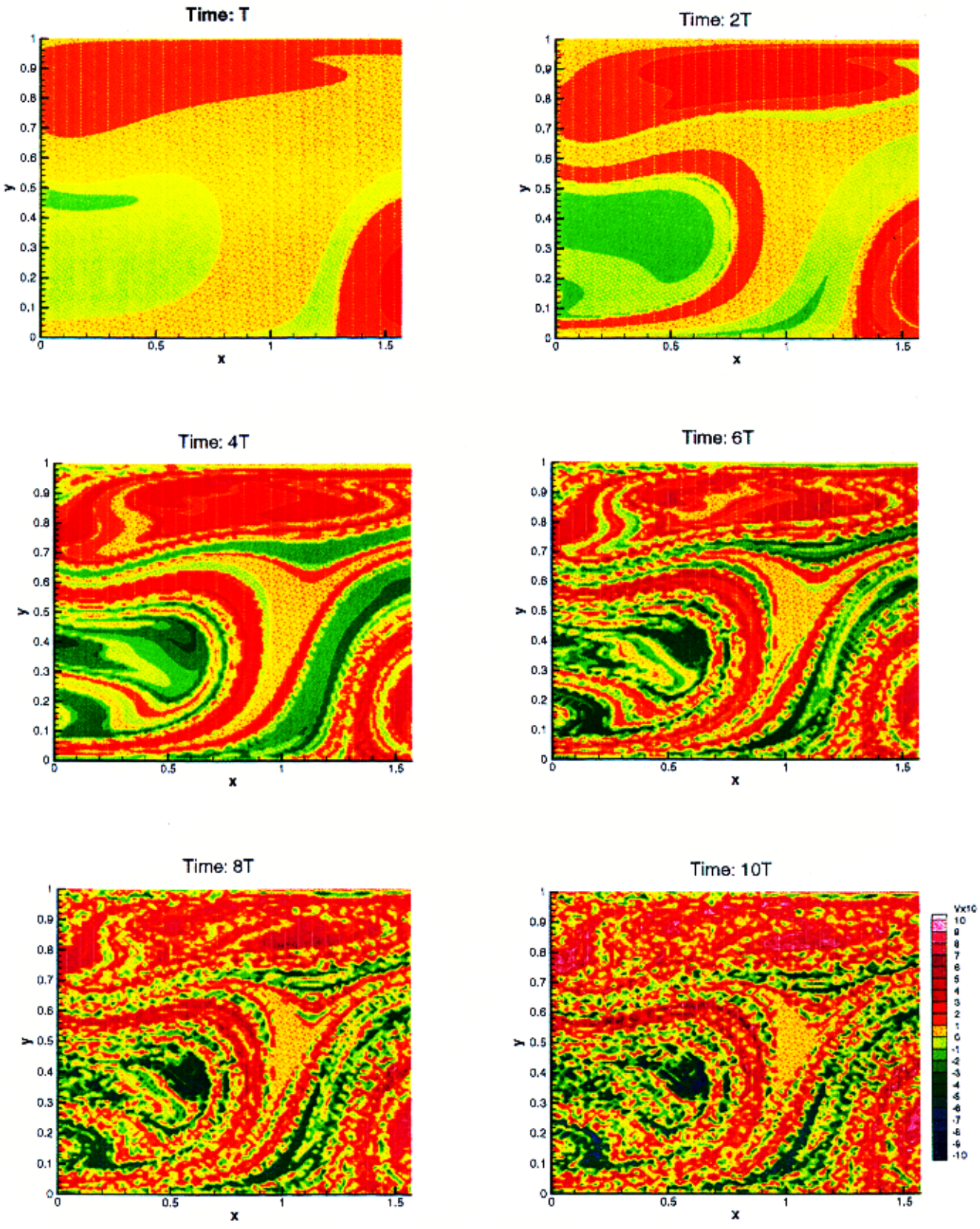

Fig. 12. (*Continued*)

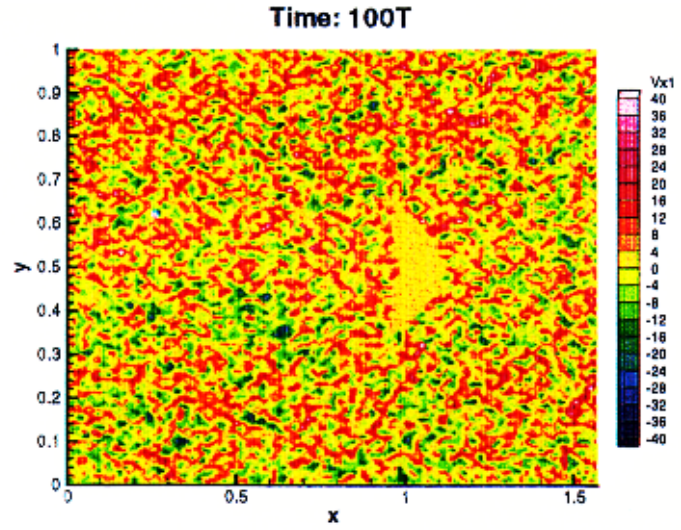

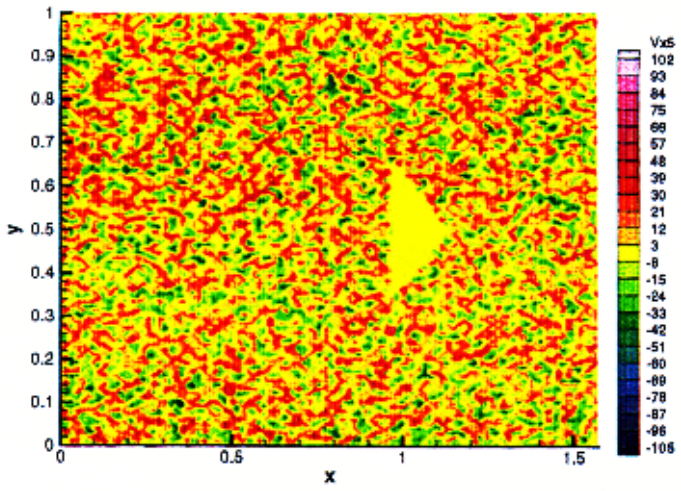

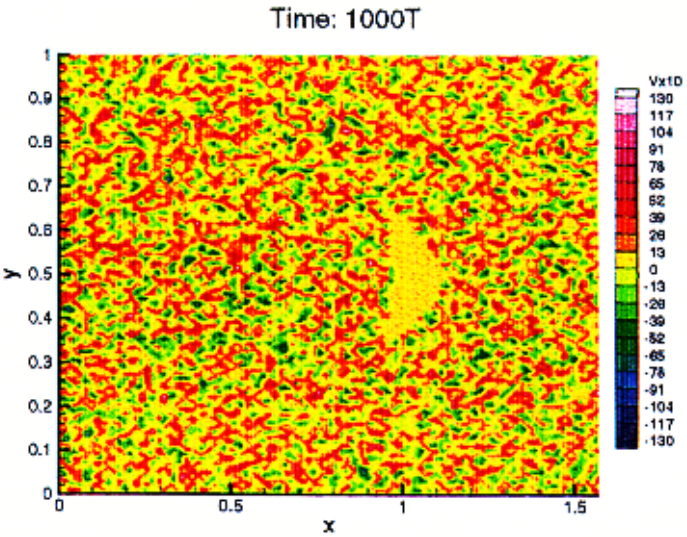

Fig. 12. (*Continued*)

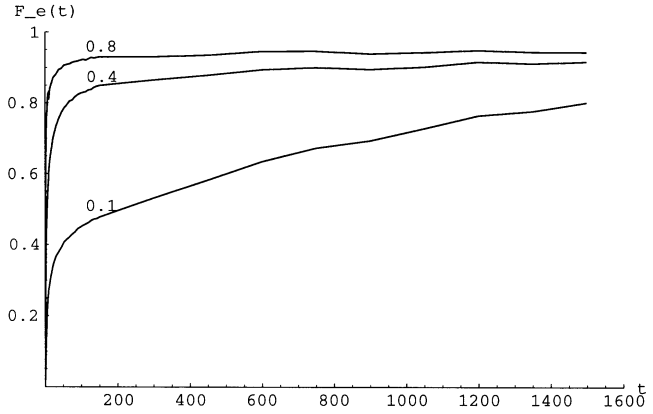

Fig. 13. The ratio of the trajectories F_e, which escape the initial cell R_0 through the left or right boundary, is shown as a function of time for up to 1000 time-periods. The curves are labeled with the respective ε values.

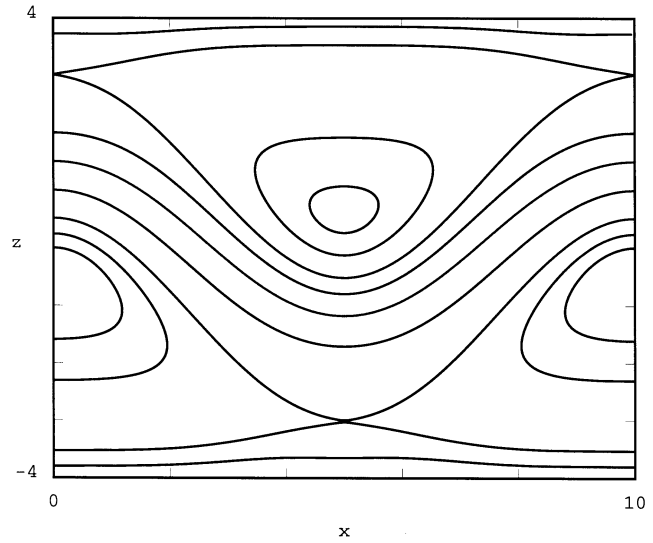

Fig. 14. Steady flow of the meandering jet as observed in a frame moving with the phase-speed of the meander. The parameters of the kinematic model are set at $B = 1.2$, $k = 0.1$, and $c = 0.1$.

co-moving with the phase-speed of the meander is given as follows.

$$\begin{aligned}\dot{x} &= -c + \frac{1}{[1+\kappa^2 B^2 \sin^2 \kappa x]^{\frac{1}{2}}} g(x,\, y) \\ \dot{y} &= \frac{1+\kappa^2 B^2(1-y\,\cos\,\kappa x)}{[2+\kappa^2 B^2(1-\cos\,2\kappa x)]^{\frac{3}{2}}} g(x,\, y)\end{aligned} \tag{20}$$

where

$$g(x,\, y) = \operatorname{sech}^2\left(\frac{y - B\,\cos\,\kappa x}{[1+\kappa^2 B^2 \sin^2 \kappa x]^{\frac{1}{2}}}\right).$$

Following [Samelson, 1992], we fix the parameters for the underlying meandering jet as $B = 1.2$, $L = 10$, and $c = 0.1$. The streamlines for the steady jet are shown in Fig. 14 in the co-moving frame. As mentioned earlier, the steady flow consists of three regular flow regimes, i.e. eastward moving fluid trajectories in the central jet, trajectories executing periodic motion above and below the central jet, and westward moving fluid trajectories exterior to the jet. The periodic motion is separated from the unbounded eastward and westward motion by a pair of heteroclinic connections which join saddle-type stagnation points.[6]

3.1. *Effect of quasi-periodic disturbances*

We examine the effect of spatially uniform quasi-periodically time-varying meridional flow over the underlying meandering jet. The resulting stream function is expressed as

$$\begin{aligned}\Phi(x,\, y,\, \tau) &= \phi(x,\, y) + \varepsilon\phi'(x,\, y,\, t) \\ &= \phi(x,\, y) + \varepsilon x \sum_{i=1}^{l} \gamma_i \cos\,(\omega_i \tau + \delta_i)\end{aligned} \tag{21}$$

where γ_i, ω_i, and δ_i are the amplitude, frequency and the phase-lag associated with the ith component of the quasi-periodic variability. For the sake of simplicity we consider only two frequencies in the disturbance.[7]

3.2. *Horizontal transport*

In order to examine the horizontal (eastward) transport in the meandering jet, we proceed in a manner similar to the cellular transport case. We consider a domain ($x \in [0,\, 10]$, $z \in [-4,\, 4]$) which contains a complete heteroclinic structure above the trough of the central jet (see Fig. 14). Next, we cover this domain with a uniform grid of 200×200 grid points. The average x-velocity contours are shown on this initial grid (see Fig. 15).

[6] "Stagnation point" is the fluid mechanical term for an equilibrium point of a steady vector field.

[7] The term "meridional flow" means that the perturbation is solely in the y direction, i.e. from the point of view of the earth, it is in the direction of the meridians.

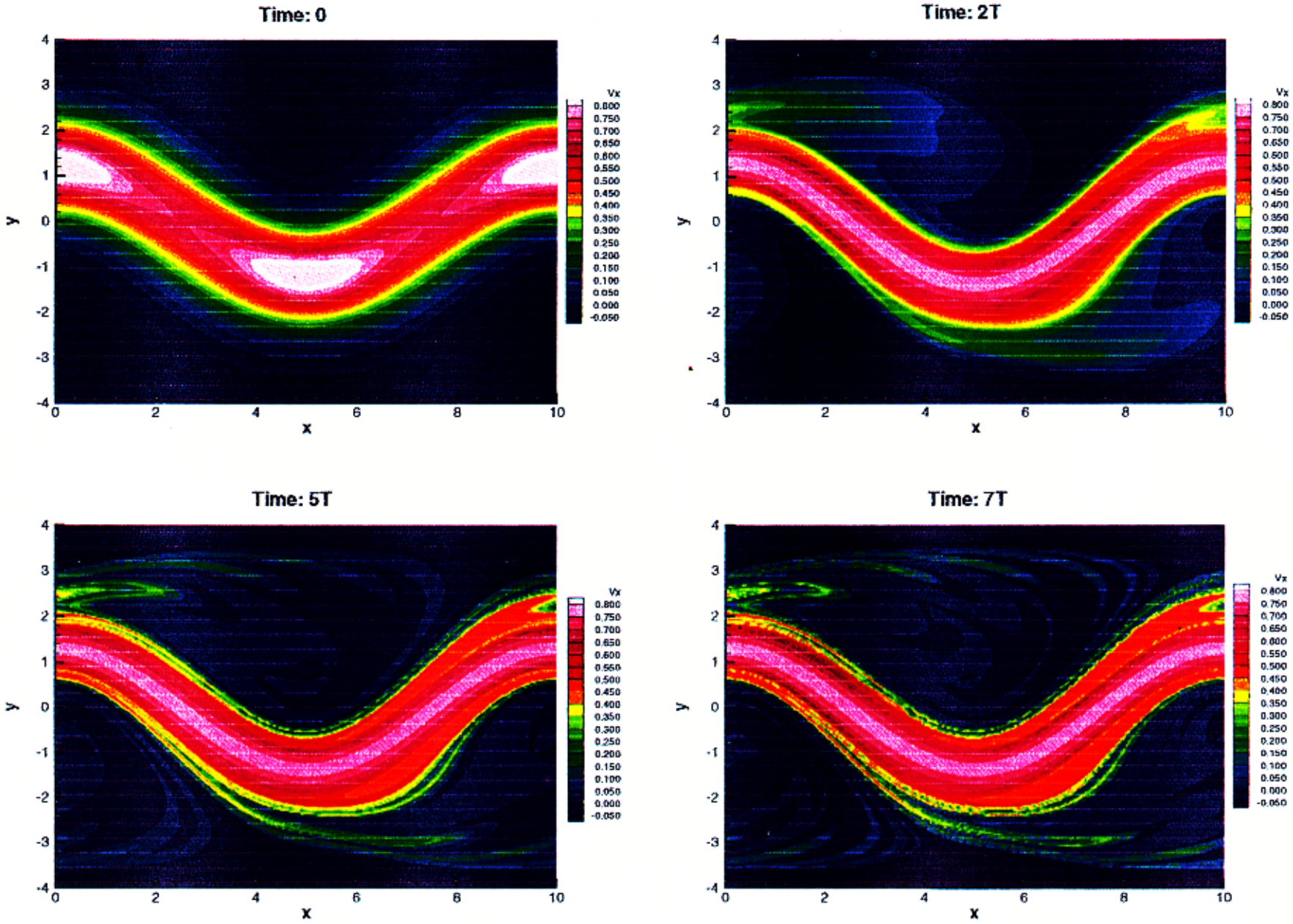

Fig. 15. Average x-velocity contours corresponding to initial points having the same time-average along the tracer trajectories at eight different time intervals. The jet parameters are fixed at $B = 1.2$, $k = 0.1$, $c = 0.1$, $\omega = (0.3, \pi)$, $\gamma = (0.5, 0.86)$, $\delta = (3.5, \pi)$, and $\varepsilon = 0.1$.

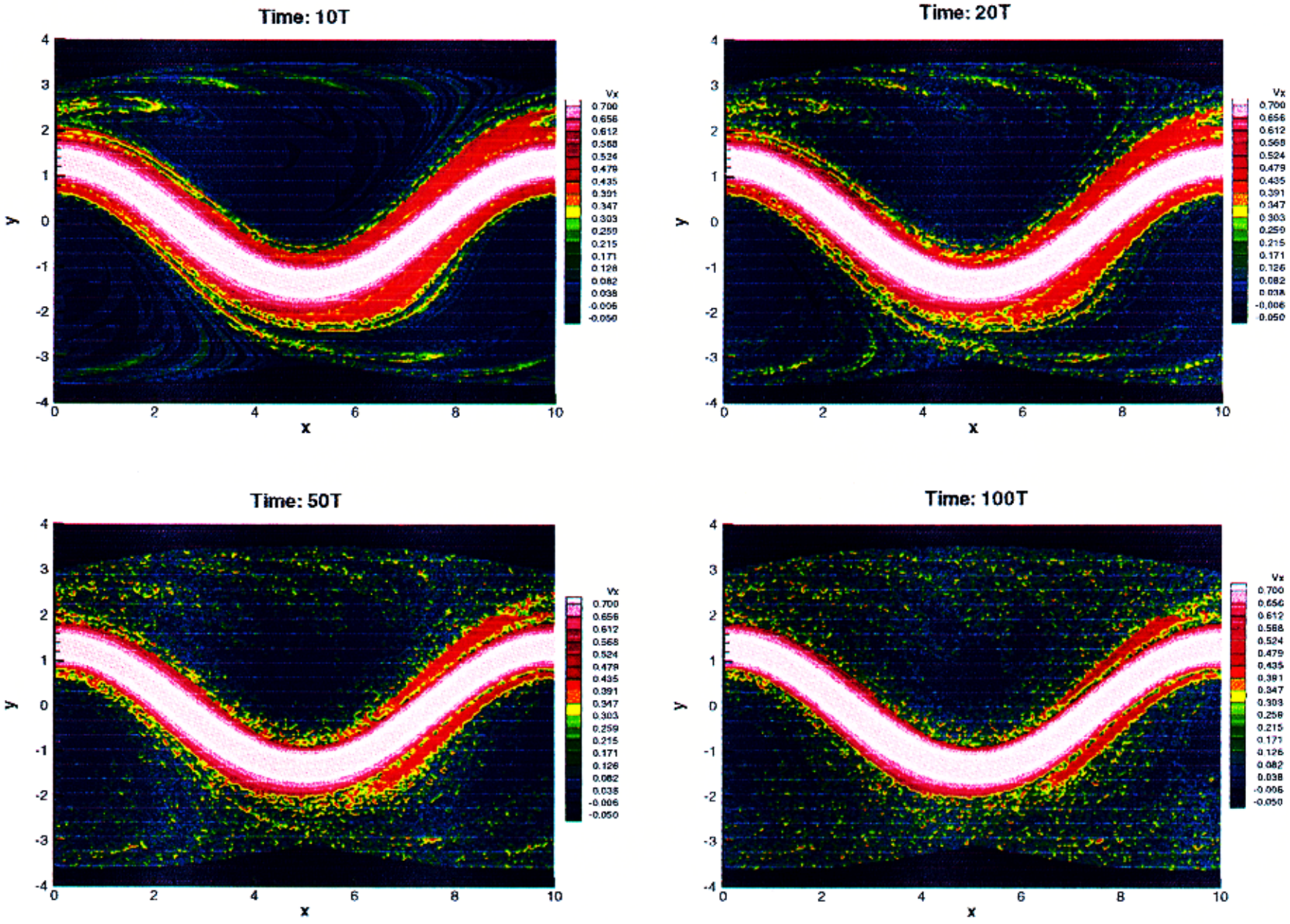

Fig. 15. (*Continued*)

3.2.1. *Description of patchiness structure*

The initial configuration of the x-velocity contours deforms along the unstable manifolds in the domain. The shape of the unstable manifolds and KAM tori appear to be well resolved in the average x-velocity plot at $5T$. As observed in the previous case, the contours start to disintegrate into big patches at first, and slowly shrink to small patches of large (as compared with the surrounding region) average x-velocity. In the case of the meandering jet flow, we observe a few distinct characteristics which distinguish the jet flow from the cellular flow.

In the meandering jet case, the domain consists of an eastward moving fast speed jet which separates the counter-clockwise periodic flow north of the central jet from the clockwise periodic flow south of the jet. For the parameter values considered here, the central jet is not affected by the time-dependence introduced due to the quasi-periodic meridional flow.

We also note the presence of two large red patches (see average x-velocity contours at later times) on the top and bottom of the central jet in the right side of the domain. The strength of these sub-regions is of a comparable magnitude to the other small patches scattered throughout the domain. These big patches arise due to the asymmetry introduced by the phase-angle parameter δ in the time-dependence.

3.2.2. *Probability distribution of patches*

The probability distribution of the patchiness is very different from the cellular flow case. In the domain considered here, the flow has a nonzero mean eastward component of velocity. In addition, the probability distribution is asymmetric about the mean flow. We notice that the distribution of the average x-component of the velocity is distinguished by the presence of four distinct peaks (see Fig. 16).

- The peak which appears close to $\langle \overline{v}_x^1 \rangle = -0.1$ corresponds to the westward moving fluid particle trajectories near the top and the bottom of the domain.

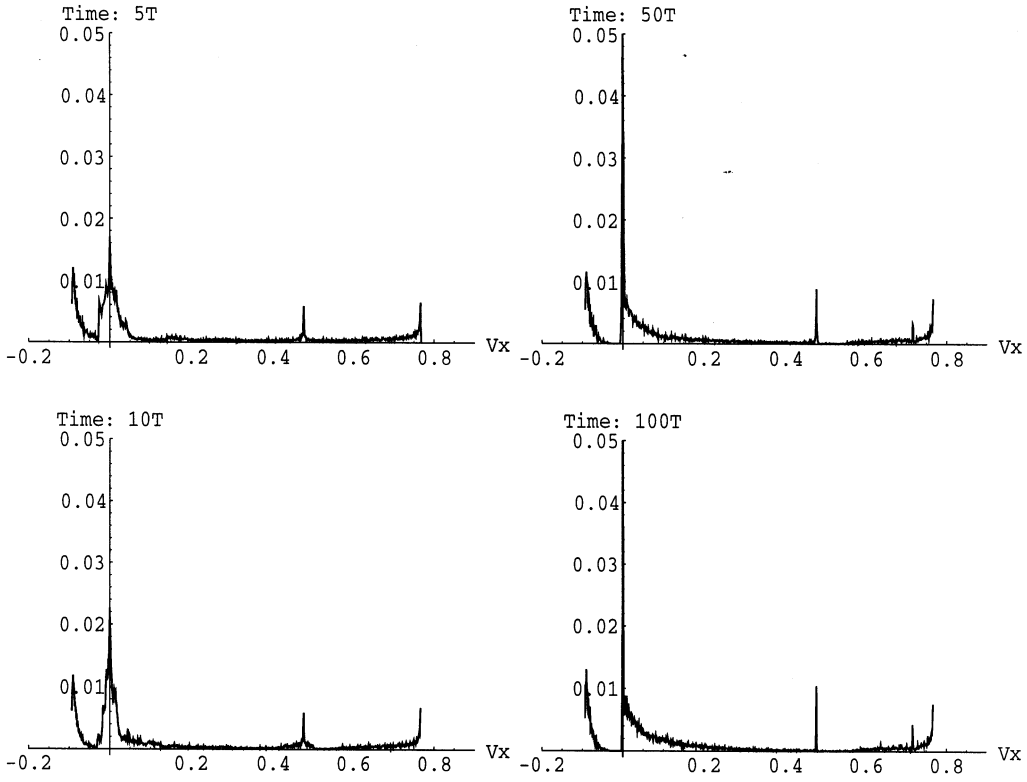

Fig. 16. The probability distribution of the averaged x-component of velocity at four different time-intervals (for perturbations arising due to the quasi-periodic meridional flow). On the vertical axis, the fraction of total points is shown. The parameters are the same as for Fig. 15.

- The largest peak at $\langle \overline{v}_x^2 \rangle = 0.0$ is due to to the background flow of very small average x-velocity.
- The peak near $\langle \overline{v}_x^3 \rangle = 0.47$ corresponds to the patches (including the two large ones) in the flow.
- The peak near $\langle \overline{v}_x^4 \rangle = 0.75$ represents the high average x-velocity of the fast moving central jet.
- At later times, we also observe the gradual appearance of new peaks between $\langle \overline{v}_x^3 \rangle$ and $\langle \overline{v}_x^4 \rangle$. These additional peaks are due to the band-like structure of the central jet region. This seems to be an important fact: While in the unperturbed case particles in the jet region were carried by a shear flow[8] with strong velocity differences between near-by streamlines, the time-dependence resulted in a formation of zones with the constant average velocity. This is the consequence of resonance-locking and the cross-section of the average-velocity profile has the structure of a devil's staircase.
- Although the peaks tend to be relatively narrower, sharper, and longer at later times, the appearance of the patchiness distribution remains the same even after $100T$ time-interval.

3.2.3. *Dispersion characteristics*

Since the probability distribution does not change appreciably with time, the dispersion of the patchiness $D_v(t)$ in the x-direction almost remains constant. This suggests asymptotic in time t^2 dispersion behavior from (8), as predicted by the general result in [Mezić & Wiggins, 1995a]. In fact, that is what we observe in the computations. Figure 17 shows the variation of the dispersion (in the x-direction) with time as $t^{1.96}$.

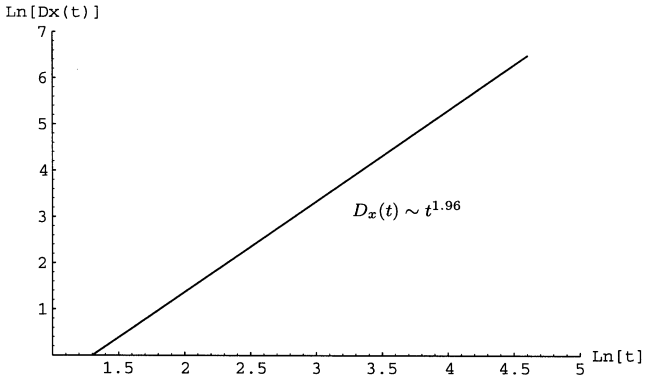

Fig. 17. Log–log plot of the $D_x(t)$ versus time for the meandering jet flow.

3.3. *Northward transport*

In the case of a meandering jet, we are also interested the northward transport of passive scalars, the interaction of the central jet with the flow above and beneath the jet, and whether there is any cross jet transport at all.

We plot the contours of the average northward velocity in Fig. 18, and probability distributions in Fig. 19. In this case, there is no net northward flow through the horizontal boundaries, and the distribution of the average northward velocity patches is symmetric about the zero mean flow and the distribution function is nearly Gaussian. The probability distribution shrinks towards the zero mean flow (in the y-direction) very fast (see Fig. 20). The corresponding dispersion of patchiness of the northward velocity decays as $t^{-1.92}$ (Fig. 21), thus indicating an extremely small growth rate of $D_y(t)$. This is due to the presence of restraints (barriers) north and south of the jet-flow.

3.4. *Comparison with time-periodic variability*

In order to compare the passive scalar transport in the quasi-periodic case with the time-periodic disturbances, we reconsider the periodic model examined by Samelson [1992]. In the case of periodically varying meridional disturbances, Samelson found that exchange across the interior heteroclinic boundaries (i.e. the boundaries adjacent to the central jet) was always greater than the exterior heteroclinic boundaries (i.e. the boundaries adjacent to the westward moving flow near the top and the bottom of the domain). This is obvious from Fig. 4 of [Samelson, 1992] which shows the behavior of the Melnikov function as the forcing frequency ω is varied from 0 to 1. On examining the transport of passive scalars for various values of the forcing frequencies, we notice that the extent to which the interior heteroclinic boundaries interact with the central jet (or the extent of interaction of the exterior heteroclinic boundaries with the westward moving flow) is directly related with the value of the Melnikov function(s) as given in Fig. 4 of [Samelson, 1992]. The patchiness behavior for four representative cases, corresponding to $\omega = 0.02$, 0.11, 0.3, and 1.0, respectively, is shown in Figs. 22–25.

[8]Roughly speaking, a "shear flow" is a flow in which the velocity is essentially in one direction, and the speed increases monotonically as one moves normal to this direction.

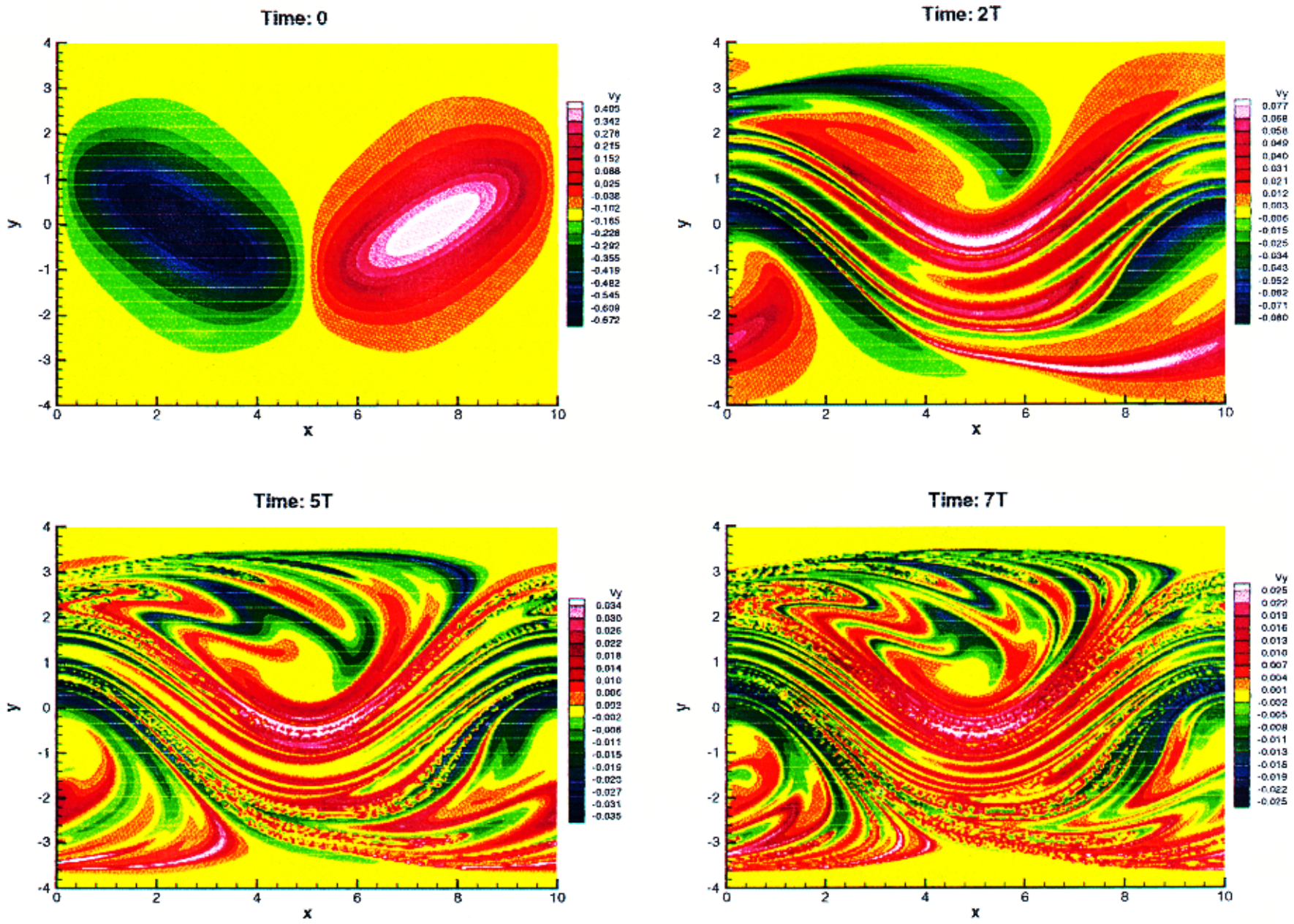

Fig. 18. Average y-velocity contours corresponding to initial points having the same time-average along the tracer trajectories at eight different time intervals. The jet parameters are fixed at $B = 1.2$, $k = 0.1$, $c = 0.1$, $\omega = (0.3, \pi)$, $\gamma = (0.5, 0.86)$, $\delta = (3.5, \pi)$, and $\varepsilon = 0.1$.

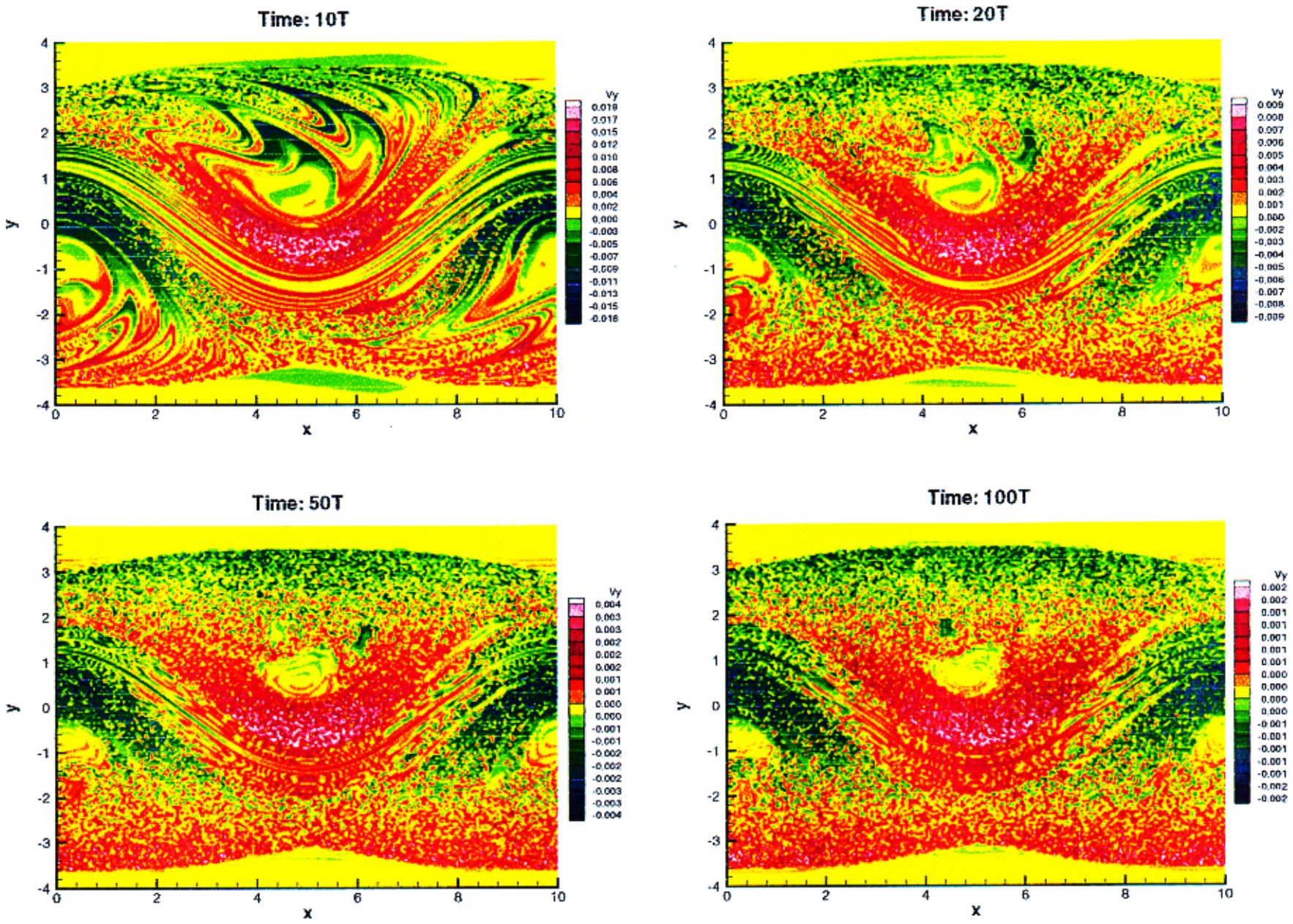

Fig. 18. (*Continued*)

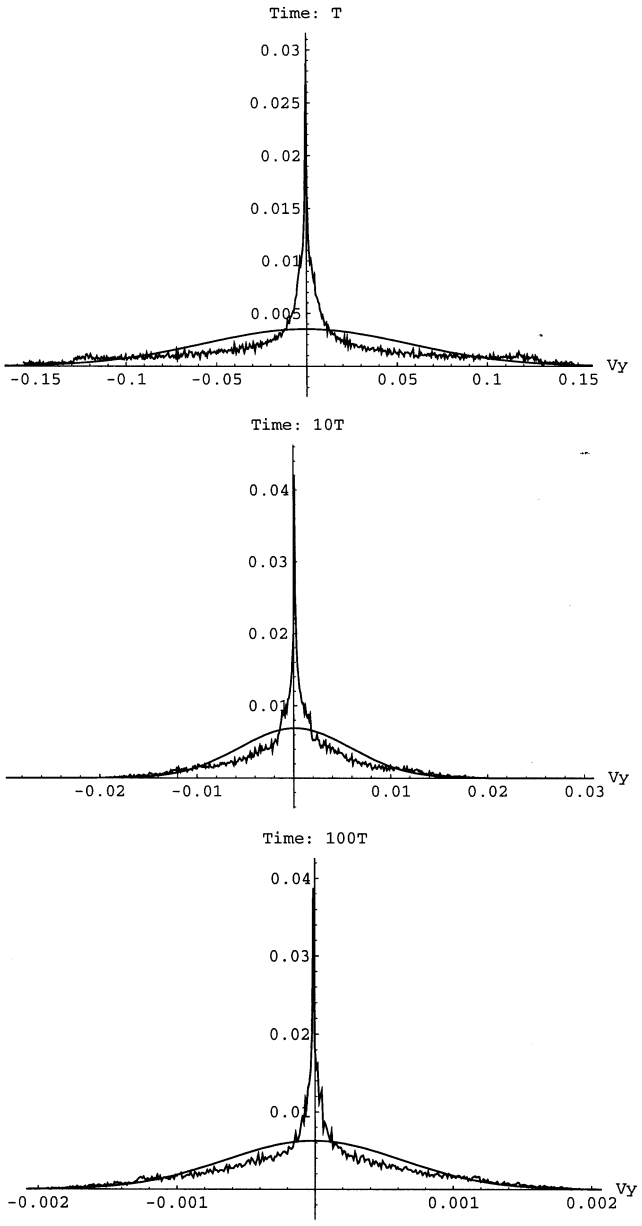

Fig. 19. The probability distribution of the averaged y-component of velocity at time T, $10T$, and $100T$. On the vertical axis, the fraction of total points are shown.

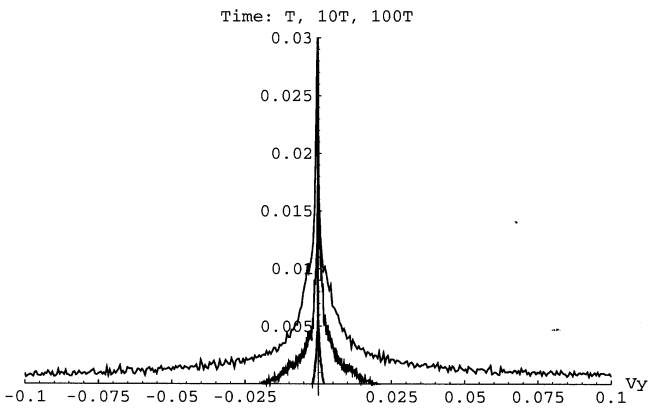

Fig. 20. Combined distribution functions for T, $10T$, and $100T$.

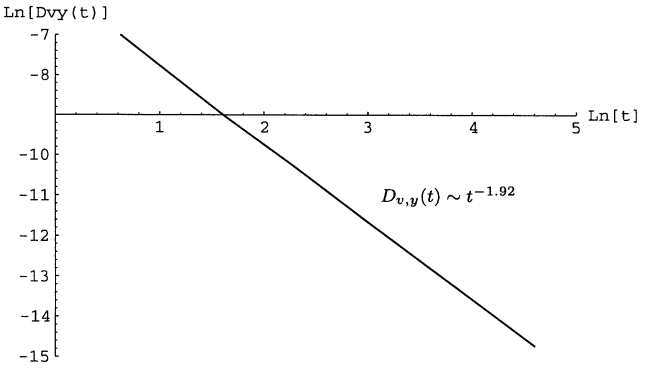

Fig. 21. Log–log plot of the $D_{v,y}(t)$ versus time for the meandering jet flow.

The first case ($\omega = 0.02$) corresponds to the largest value of the Melnikov function for both exterior as well as interior boundaries, and thus exhibits the maximum amount of transport across both boundaries (see Fig. 22). The exterior boundaries after breaking-up act to bring-in the westward moving flow in the recirculatory regime, while the interior boundaries vigorously interact with the central jet and lead to considerable amount of transport across the jet. Despite the presence of such strong interaction, we also observe the presence of two invariant sub-domains of zero transport (KAM-tori). The second case ($\omega = 0.11$) corresponds to the significantly larger transport across the interior boundaries as compared with the exterior boundaries (see Fig. 23). In this case, the initially fast moving central jet is a region filled with patches after $10T$ time-interval, while very little number of westward moving patches are observed in the domain. On increasing the value of ω to 0.3 (Fig. 24), we notice that the central jet preserves its structure even after $10T$, although narrower than the steady case. In this case, the interior boundaries primarily interact with the edges of the jet. We also notice the presence of a cluster of eastward moving patches on either side of the central jet in the right half of the domain. The last case ($\omega = 1$) corresponds to the weaker version of the previous case. Here, we only observe a fuzzy region near the heteroclinic boundaries (see Fig. 25), and elsewhere the flow is similar to the steady case.

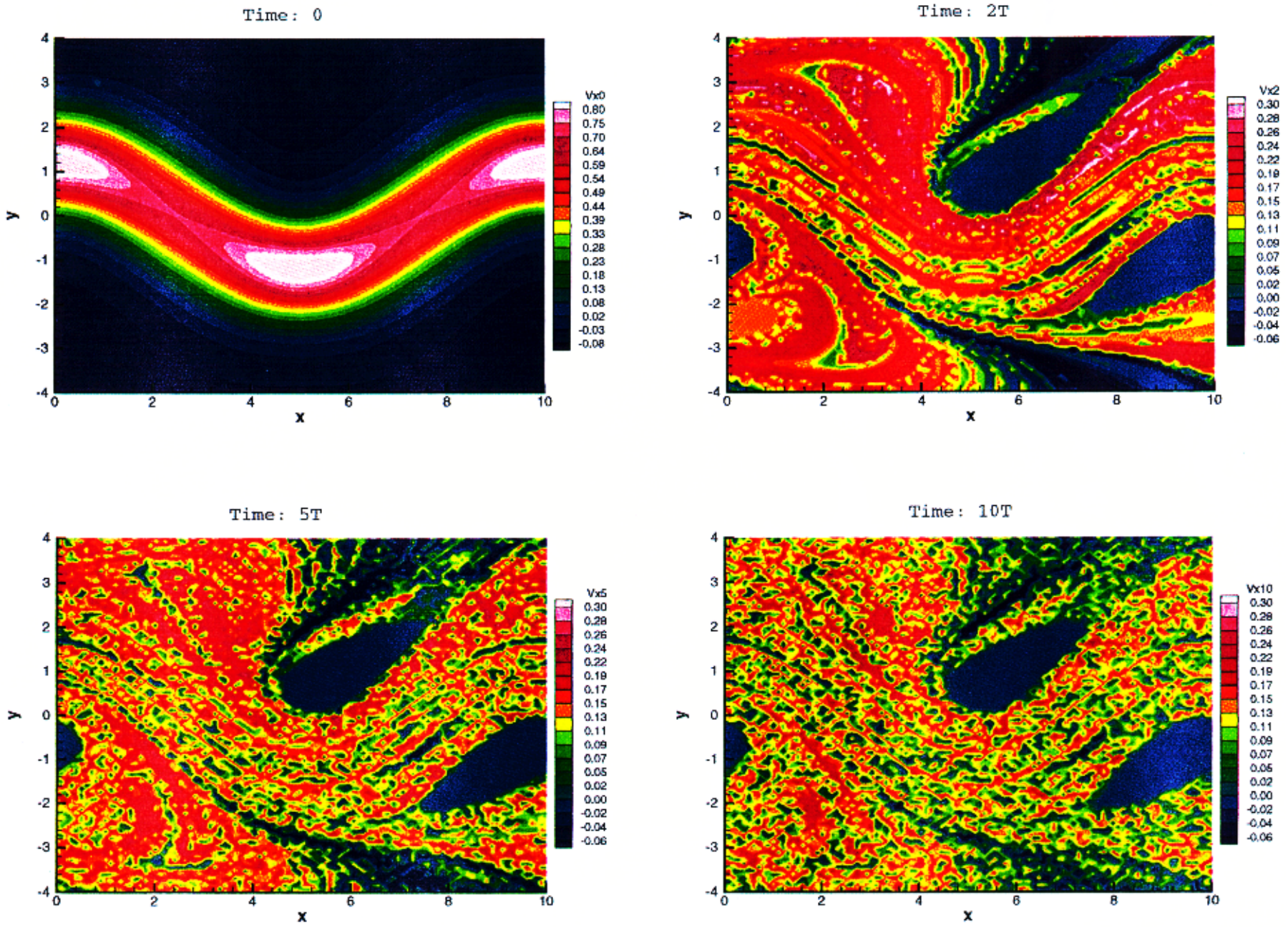

Fig. 22. Same as Fig. 15 except for the periodic case with $\omega = 0.02$, $T = 314.16$, $\delta = \pi$, and $\varepsilon\gamma = 0.1$.

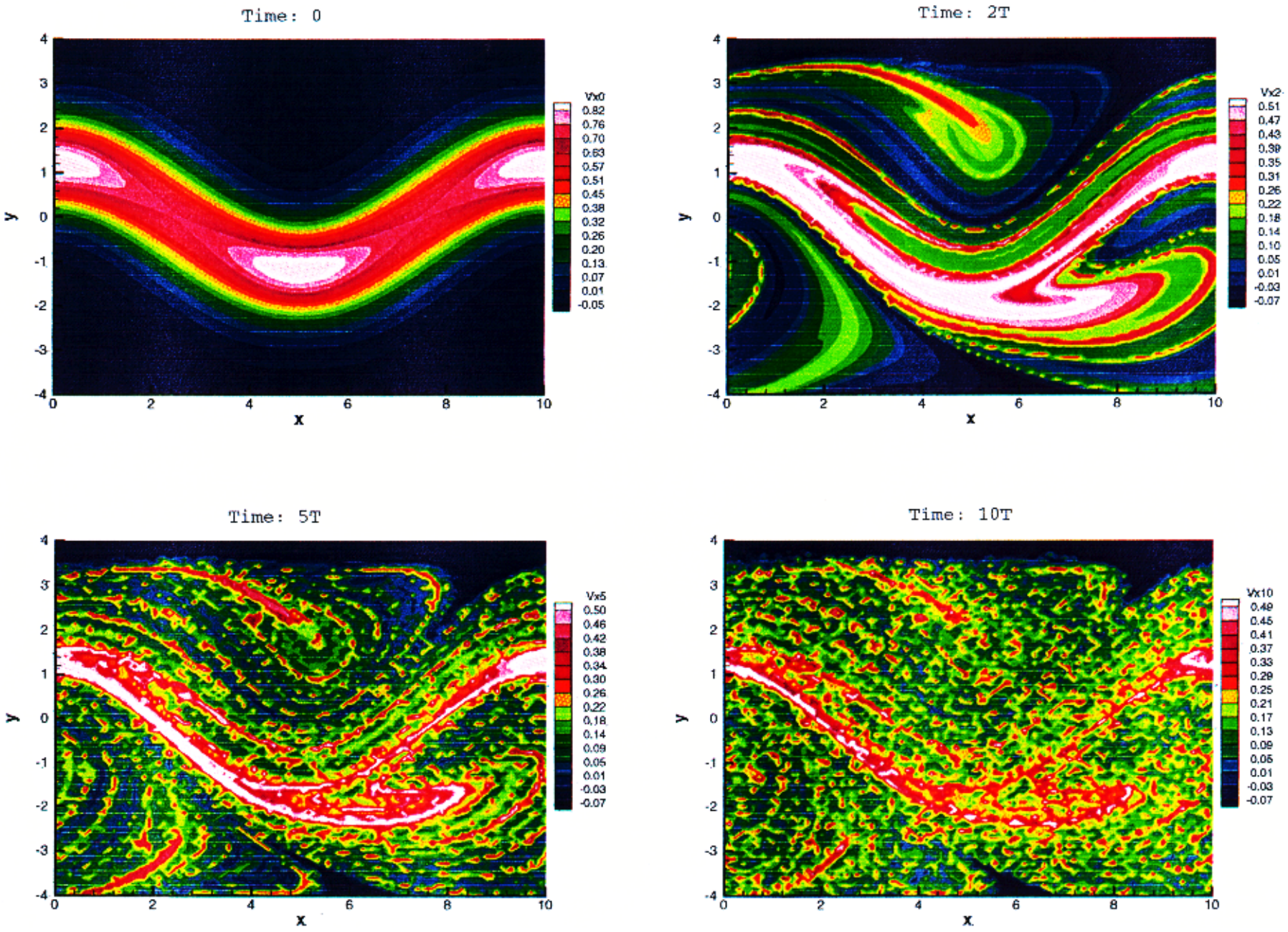

Fig. 23. Same as Fig. 22 except for $\omega = 0.11$, and $T = 57.12$.

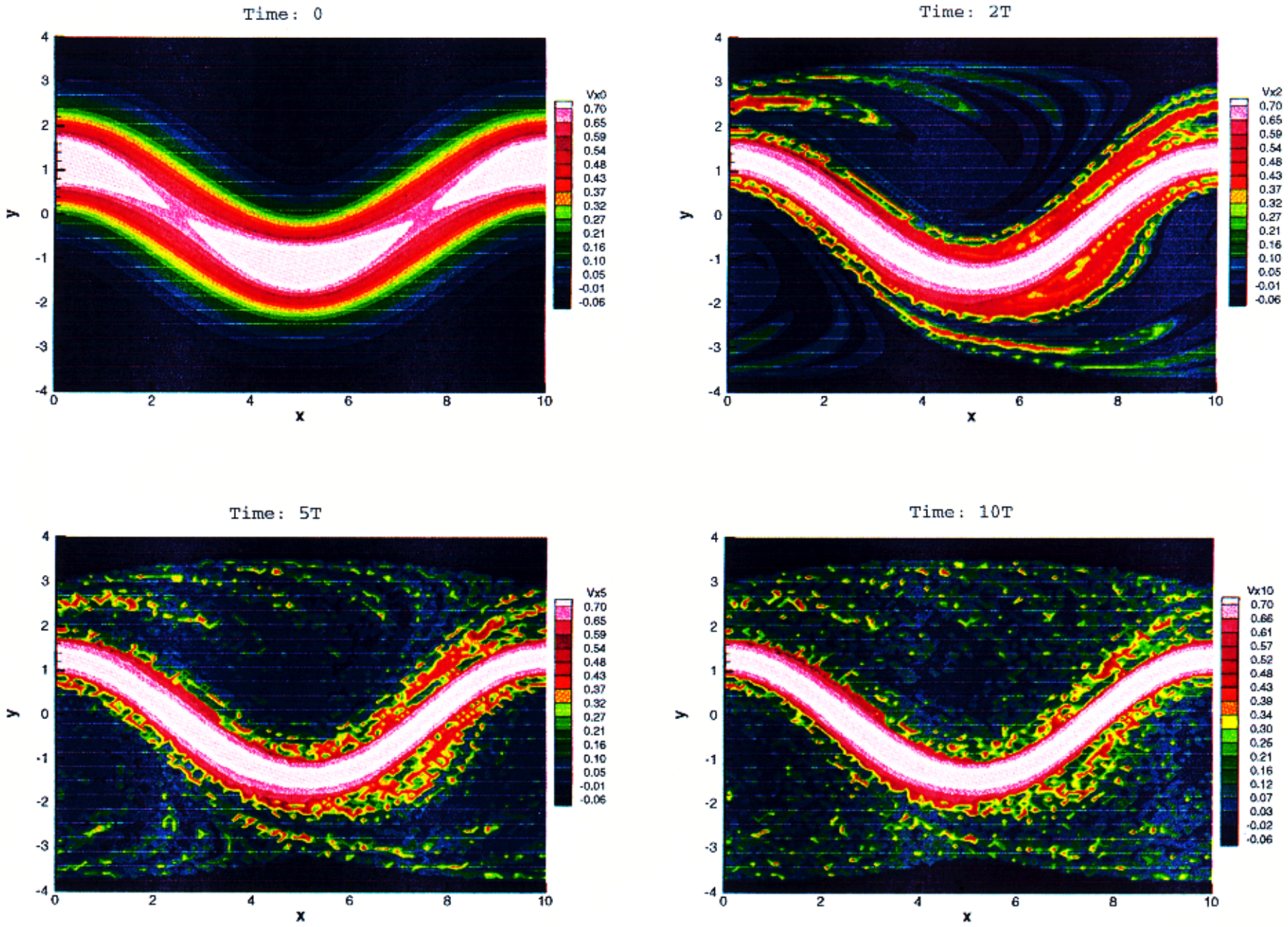

Fig. 24. Same as Fig. 22 except for $\omega = 0.3$, and $T = 20.94$.

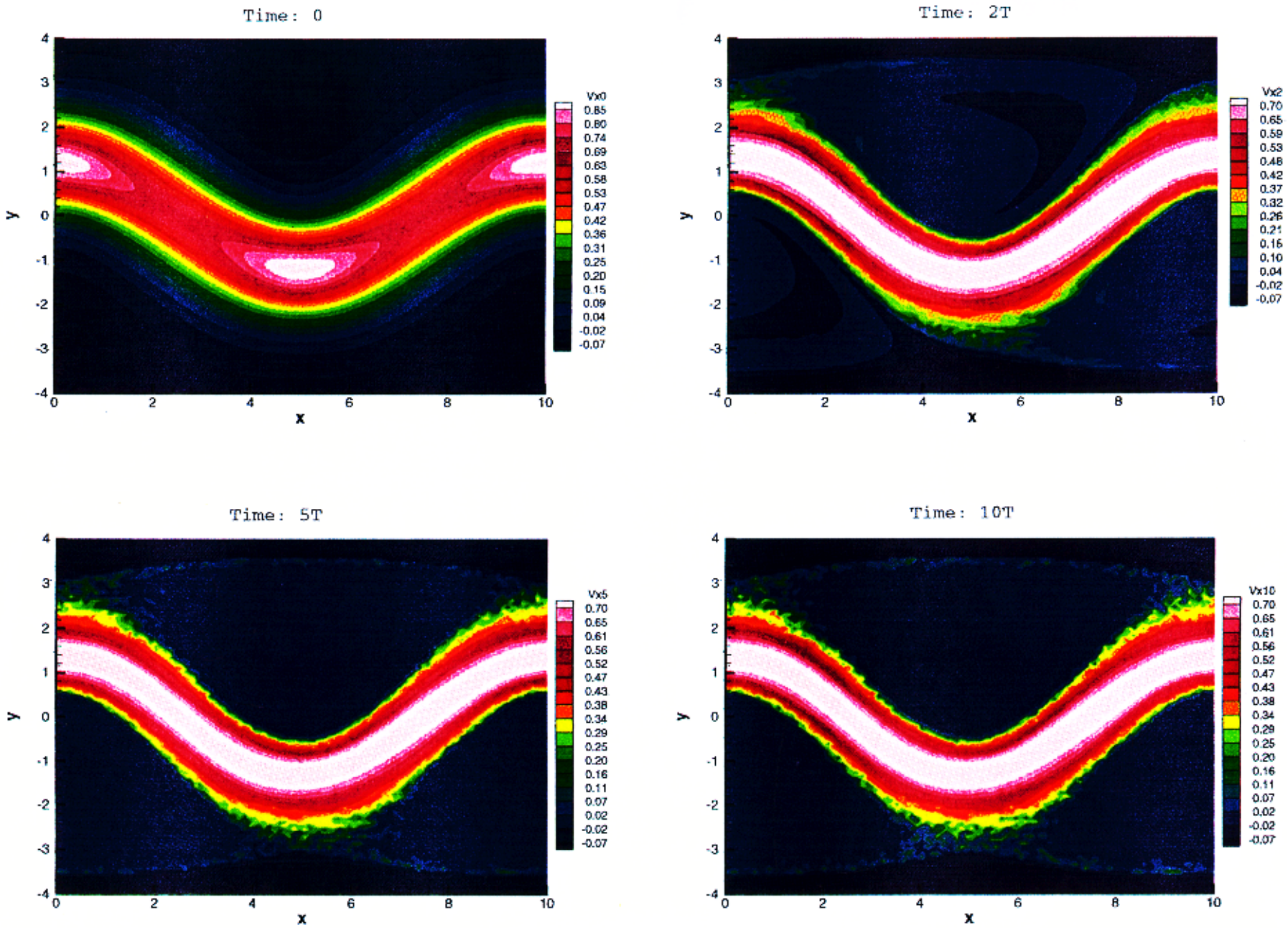

Fig. 25. Same as Fig. 22 except for $\omega = 1$, and $T = 6.28$.

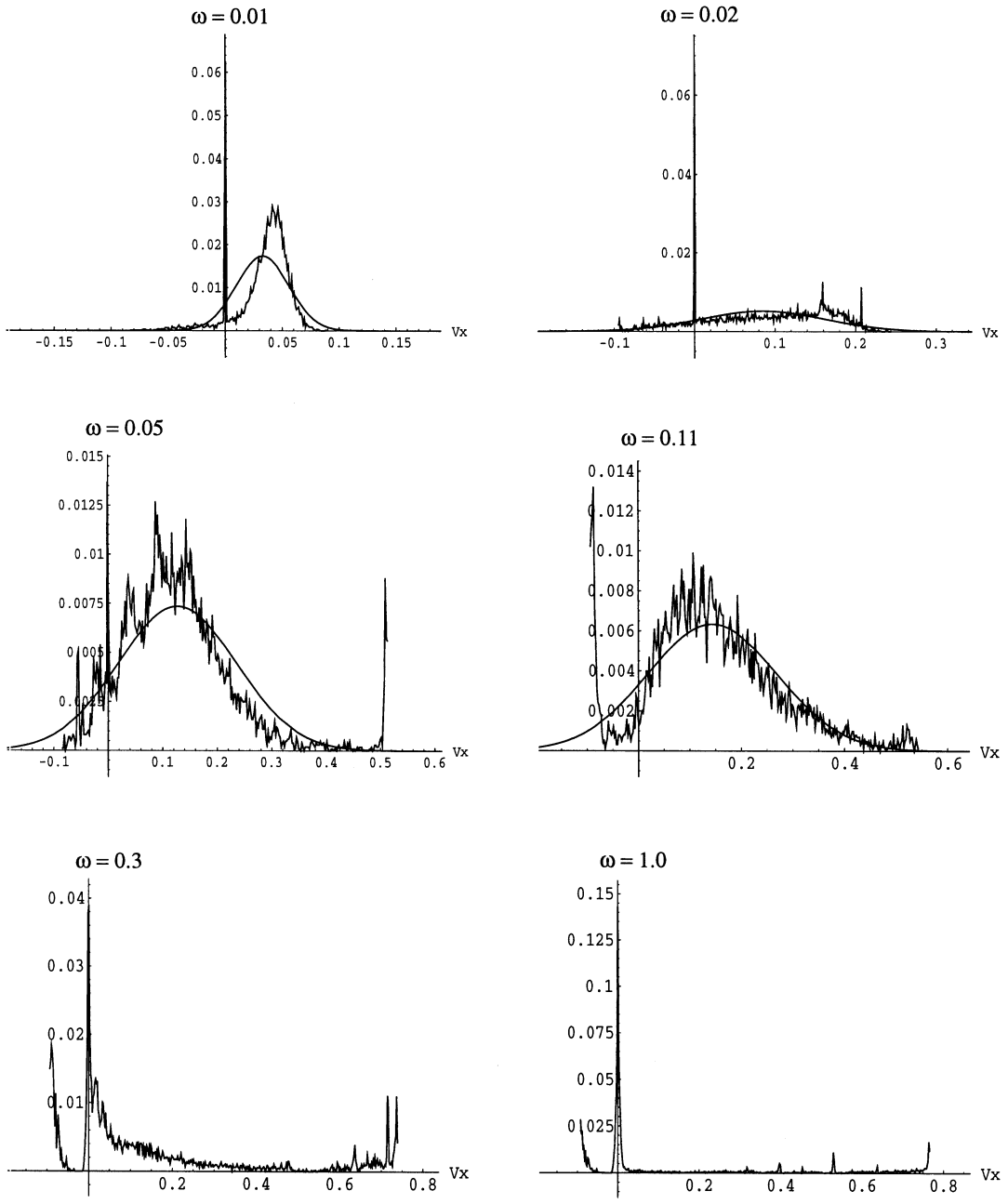

Fig. 26. The probability distribution of patchiness for various values of forcing frequency after 10 time-periods.

The probability distribution of the patches shows a variety of behavior as ω is varied from 0 to 1. We show the distribution of patchiness after 10 time-periods for six different values of the forcing frequency in Fig. 26. The probability distribution is closest to the Gaussian distribution (with eastward moving mean-flow) for $\omega = 0.11$, and for values of ω larger than 0.11 the distribution tends to be dominated by a finite number of peaks. For all values of $\omega < 0.11$, the distribution is characterized by the presence of a broad range of average x-velocities that are uniformly distributed.

The dispersion of patchiness is shown in Fig. 27 and the corresponding dispersion behavior of passive tracers is shown in Fig. 28. For $\omega = 0.01$, the dispersion law for the particle trajectories evolves like t in the beginning but eventually it settles to t^2 behavior. This case exhibits an interesting

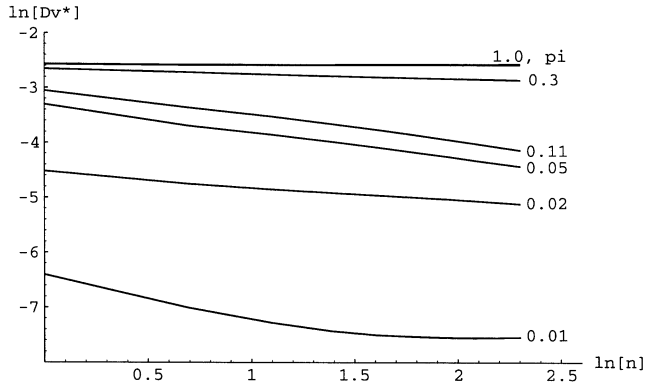

Fig. 27. The dispersion of patchiness as a function of time on a logarithmic scale. On the vertical axis, we plot $D_v^* = D_v(t)/T^2$, where $T = 2\pi/\omega$, and along the horizontal axis $n = t/T$ is shown. The different curves are labeled with the corresponding frequency values (ω).

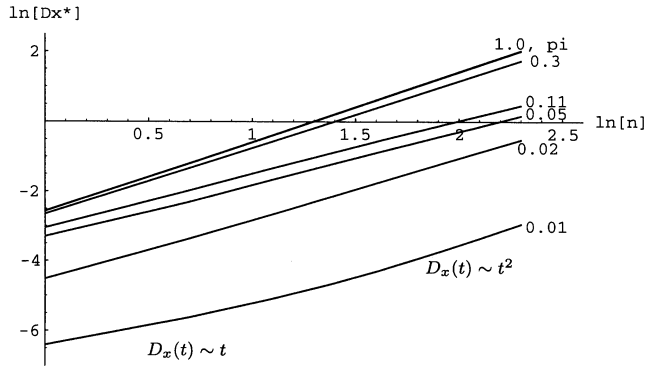

Fig. 28. Same as Fig. 27 except the dispersion of passive tracers $D_x^* = D_x(t)/T^2$ is shown along the vertical axis.

Table 1. The patchiness and passive particle dispersion exponents for various ω-values.

Frequency (ω)	γ	γ_x
0.01	0.0	2.0
0.02	−0.2	1.8
0.05	−0.5	1.5
0.11	−0.6	1.4
0.15	−0.1	1.9
0.3	−0.1	1.9
1.0	0.0	2.0
π	0.0	2.0

$t^2 \to t \to t^2$ dispersion behavior.[9] The passive particle dispersion exponent γ_x sharply decreases to 1.4 for $\omega = 0.11$, and then approaches the ballistic behavior ($\gamma_x = 2$) very fast. Table 1 gives the exponents corresponding to different values of ω after 10 time-periods.

4. On the Evolution of Patchy Structures

In the previous sections we observe that the patchy structures prominently govern the Lagrangian transport of the passive particle trajectories. However, the following questions remain unanswered.

- How do such structures evolve?
- What is the nature of their existence?
- Why do certain spatial locations within the domain lead to the formation of patches while others do not?

The answers to these questions are obtained by relating the patchiness behavior with the geometrical characteristics of the underlying flow.

4.1. *Stable and unstable manifolds*

We recall that both the flows examined in the present study have a strong hyperbolic component in the sense that they contain hyperbolic trajectories whose stable and unstable manifolds intersect transversely to give chaotic, hyperbolic invariant sets. It is well known that the stable and unstable manifolds of hyperbolic periodic orbits present in the flow provide the basic geometric templates for the study of the transport behavior (see e.g. [Wiggins, 1992]). It is generally not possible to derive analytic expressions for the stable and unstable manifolds, and thus we resort to numerical computations. For periodic time-dependence, the most widely used numerical algorithms involve finding a small segment of the stable (unstable) manifold near the saddle point, evolving this segment under the velocity field, and mapping the flow at every time-period. However, for quasi-periodic and aperiodic time-dependence one can use *double time-slice*

[9]In the theory of turbulent dispersion, it is well known that the mean square distance of the particles $D_{\text{turb}}(t)$ at time t varies like t^2 for $t \ll 1$. Mezić [1994] uses Wiener's local ergodic theorem to show initial behavior of $D(t)$ as t^2 for the velocity fields such as the ones discussed in this paper (the interested reader is referred to Theorem 3.5.2 in [Mezić, 1994]).

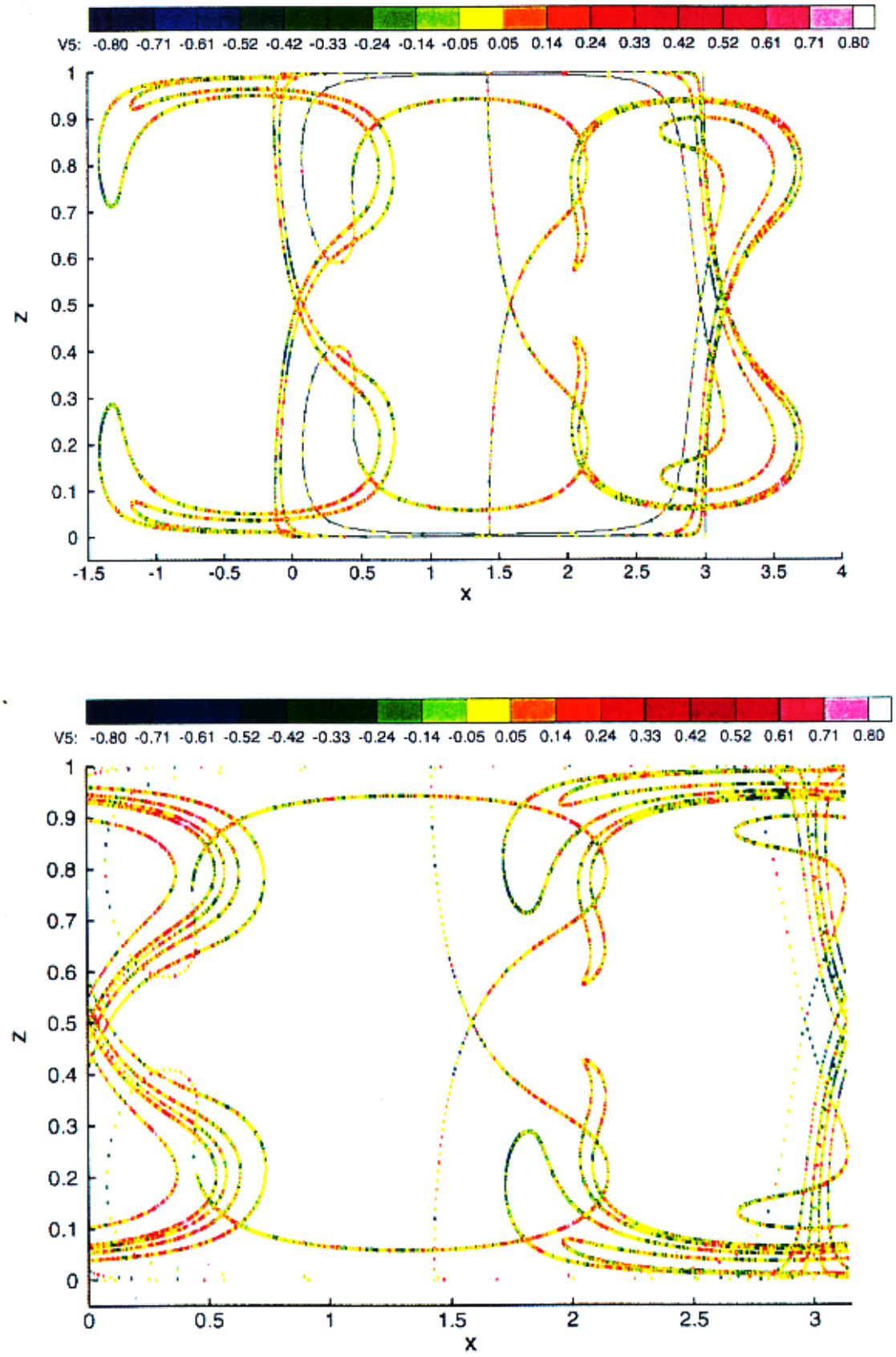

Fig. 29. Average x-velocity (shown in color) corresponding to the tracer particles lying on the stable and unstable manifolds associated with Rayleigh–Bénard flow. The parameters are fixed at $A = 1$, $k = 2$, $\omega = 4.2$, and $\varepsilon = 0.1$.

method. This method involves initializing a small geometric object surrounding the hyperbolic point on two different time-slices ($\Sigma_{T-\Delta T}$, and $\Sigma_{T+\Delta T}$, respectively), and evolving such an object forward and backward to the intermediate time-slice Σ_T. We refrain from providing the details of algorithm to compute the manifolds, and refer the reader to [Parker & Chua, 1989] for the time-periodic case, and [Malhotra & Wiggins, 1998] (and references therein) for the *double time-slice method* used for quasi-periodic/aperiodic time-dependence.

In two-dimensional time-dependent velocity fields, the stable and unstable manifolds intersect to form lobes on any time-slice and these lobes act as primary agents of the fluid transport (see [Wiggins, 1992]).

4.2. *Patchiness structures as geometric constructs*

In the cellular transport case, the manifolds are computed for a reference case, and are shown in Fig. 29. These stable and unstable manifolds are computed for up to two time-periods for the sake of clarity of the intersections, and the adequate resolution for the manifolds. For periodic time-dependence, we notice that all lobes occupy the same area in the fluid domain. In order to gain an understanding of the behavior of particle trajectories at longer times, we also compute the average x-velocity for 10 000 points lying on each of the stable and unstable manifolds. The average x-velocity is shown in various colors in this diagram. We observe an interesting behavior of the average x-velocity spectrum along the manifolds. We notice unusually high magnitude of average x-velocity values along the boundaries of the secondary lobes (i.e. the lobes formed by the intersection of primary lobes). Along the boundaries of primary and secondary lobes, we also notice a spectrum of colors which signify the additional higher order manifold intersections after we compute the additional length of manifolds beyond $\Delta T = 2T$. On comparing the location of these secondary and higher order lobes, we recognize that such locations approximately correspond to the location of the patches in a cell.

We use the *double time-slice method* to compute the manifolds for the meandering jet with quasi-periodic meridional flow (see Fig. 30). We compute the manifolds for the flow above the central jet only, because the rest of the flow-picture can be constructed from symmetry arguments. In this case, the manifolds are computed in such a way that the trajectories re-enter the domain (because of spatial periodicity in x-direction). This way we are able to compute the manifolds for $\Delta T = 10T$ with reasonable resolution. For the sake of clarity we show the stable and unstable manifolds separately. Once again, we calculate the average x-velocity spectrum for 10 000 points along the manifolds. It is easy to discern unusually high average x-velocity values along the boundaries of secondary lobes. We can also isolate the boundary of the large patch as seen earlier in corresponding patchiness plot (see Fig. 15).

In both the cases described here we notice that overlapping segments of the lobe area are the regimes of higher average velocity or patches. Since such a patchy area lies on two lobes moving in two different time-directions, and thus this area is capable of transporting itself along the unstable direction ($t > 0$) and the stable direction ($t > 0$) with equally high magnitude of x-average velocity.

5. Effect of Molecular Diffusivity

We have thus far seen the effect of periodic/quasi-periodic time-dependence on the fluid transport across the boundaries. Under such deterministic time-dependence (periodic or otherwise), the fluid transport through lobes dominates for a long time if the molecular diffusion coefficient of the passive scalar is small, but in the limit $t \to \infty$ the molecular diffusion would definitely have an impact on the transport and mixing properties of the fluid particles. Camassa and Wiggins [1991] provides a criterion which enables us to determine a time-scale beyond which the molecular diffusion may have significant impact on the transport properties. This states that the fluid transport via lobes would dominate over the molecular diffusion provided the time-scale for a passive particle to diffuse across a distance of the order of a turnstile width, T_d, is long compared to the time T for the turnstile to be mapped across the roll boundary.

Now we address the problem of transport in the presence of molecular diffusion. Such random perturbations may be introduced through thermal or turbulent fluctuations in the velocity field. It is easy to show that in the Lagrangian description, a small random process term in the velocity field (2) is equivalent to the molecular diffusion in the Eulerian approach (see e.g. a classic review by

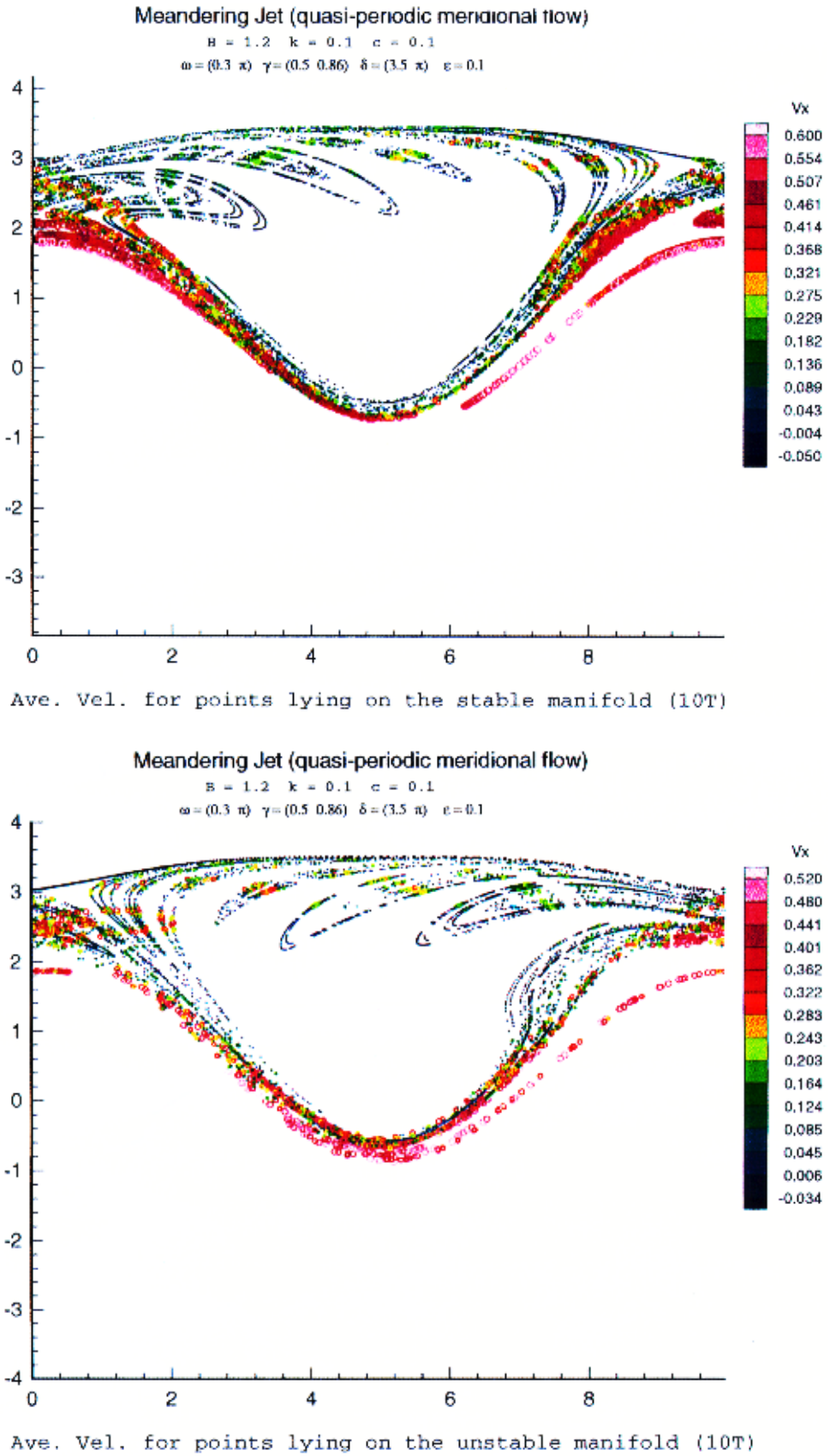

Fig. 30. Average x-velocity (shown in color) corresponding to the points lying on the stable and unstable manifolds associated with the meandering jet. The jet parameters are fixed at $B = 1.2$, $k = 0.1$, $c = 0.1$, $\omega = (0.3, \pi)$, $\gamma = (0.5, 0.86)$, $\delta = (3.5, \pi)$, and $\varepsilon = 0.1$.

Chandrasekhar [1943], or a recent review by Crisanti *et al.* [1991]). The resulting motion of the tracer particles is described by a generalized Langevin equation,

$$\begin{aligned} \dot{x} &= -\frac{\partial \psi}{\partial z}(x,\, z,\, t) + \eta_x(t)\,, \\ \dot{z} &= \frac{\partial \psi}{\partial x}(x,\, z,\, t) + \eta_z(t)\,, \end{aligned} \tag{22}$$

where $\eta_x(t)$ and $\eta_z(t)$ are two homogeneous and isotropic random processes with Gaussian probability function of zero mean and the following correlation properties.

$$\begin{aligned} \langle \eta_x(t)\eta_x(t')\rangle = \langle \eta_z(t)\eta_z(t')\rangle = 2\nu\delta(t-t')\,, \\ \langle \eta_x(t)\eta_z(t')\rangle = 0\,, \end{aligned} \tag{23}$$

where ν is the associated molecular diffusity.

Here, we are mainly interested in what happens to the patchiness structure (both, geometrically as well as probabilistically) in the presence of small but finite value of ν. For this we consider a cell filled with 100×100 passive tracers which are uniformly distributed throughout the cell at $t = 0$. The cell parameters are fixed at $A = 0.5$, $\varepsilon = 0.2$, $\omega = 4.2$, and the passive particles are assumed to have a molecular diffusion coefficient $D = 10^{-4}$. For these values, using the results in [Camassa & Wiggins, 1991], we can easily show $T_d \approx 24T$. Thus, we would expect the molecular diffusion to significantly impact the passive scalar transport beyond $24T$. This is what we observe in the patchiness plots. Figure 31 shows the x-average velocity contours for the deterministic and random cases for three different time-intervals from $25T$ to $50T$. The main feature which we identify is the presence of a 1:5 resonance band, and a large KAM torus located in the central part of the cell. A careful comparison of the two diagrams reveals that most of the patchy structures, which are located at the boundary between the large KAM torus in the center and the 1:5 resonance band, leak out to the surrounding area. The particle trajectories, originating inside these patches, drift towards other nearby trajectories as a result of random perturbations. These new trajectories have different patchiness properties due to inherent spatial inhomogeneities in the velocity field. These features are most pronounced in the slice at $t = 50T$. The main observations are as follows.

- The patches located at the boundary between the resonance bands, KAM tori, or other invariant regions in the phase space erode much faster as compared with the patches which co-exist in a dense patchy region. This is because the difference of the x-average velocity component between such patches and the surrounding region is much larger, and the passive tracers (which initially have large x-average velocity) have to traverse a very small distance to get onto the trajectories with almost negligible x-average velocity.
- As these patches erode, at first the external boundary reaches out to the outside flow, and the patch diminishes towards the smaller and smaller core region before completely disappearing into oblivion.
- The trajectories originating from other patches can also leap out either to the ambient region or to other patches, and as a result such patches also erode, but with a much slower rate.
- At the same time the trajectories originating from the outside region can also land up in a patchy region but with much less probability because by definition the patches are localized regions in the space.
- We recall that the probability distribution of cell patchiness is Gaussian even in the presence of periodic time-dependence, and thus the addition of white noise does not make any striking difference. However, the erosion of boundary patches is evident because of a larger peak near the zero x-average velocity as a result of random perturbations.

For the jet transport case, we consider the effect of random noise in the presence of periodic excitation with $\omega = 0.3$ while fixing other jet parameters to be the same as those considered in Sec. 3. For $\varepsilon\gamma = 0.1$, and $D = 5 \times 10^{-3}$, using the results in [Camassa & Wiggins, 1991] we can numerically obtain $T_d \approx 20T$. The corresponding patchiness structure is shown in Fig. 32 for the purely periodic as well as with random noise added in the velocity field. In this case we notice the presence of a cluster of patches above and below the central jet mainly in the right half of the domain. We notice that the isolated patches (such as one that are far away from the central jet) tend to grow smaller in size, while their boundaries erode as particle trajectories originating in them tend to escape towards the background flow region of different patchiness properties. But the patches in the vicinity of the central jet can also grow in strength and size as the originating particle trajectories have an equally

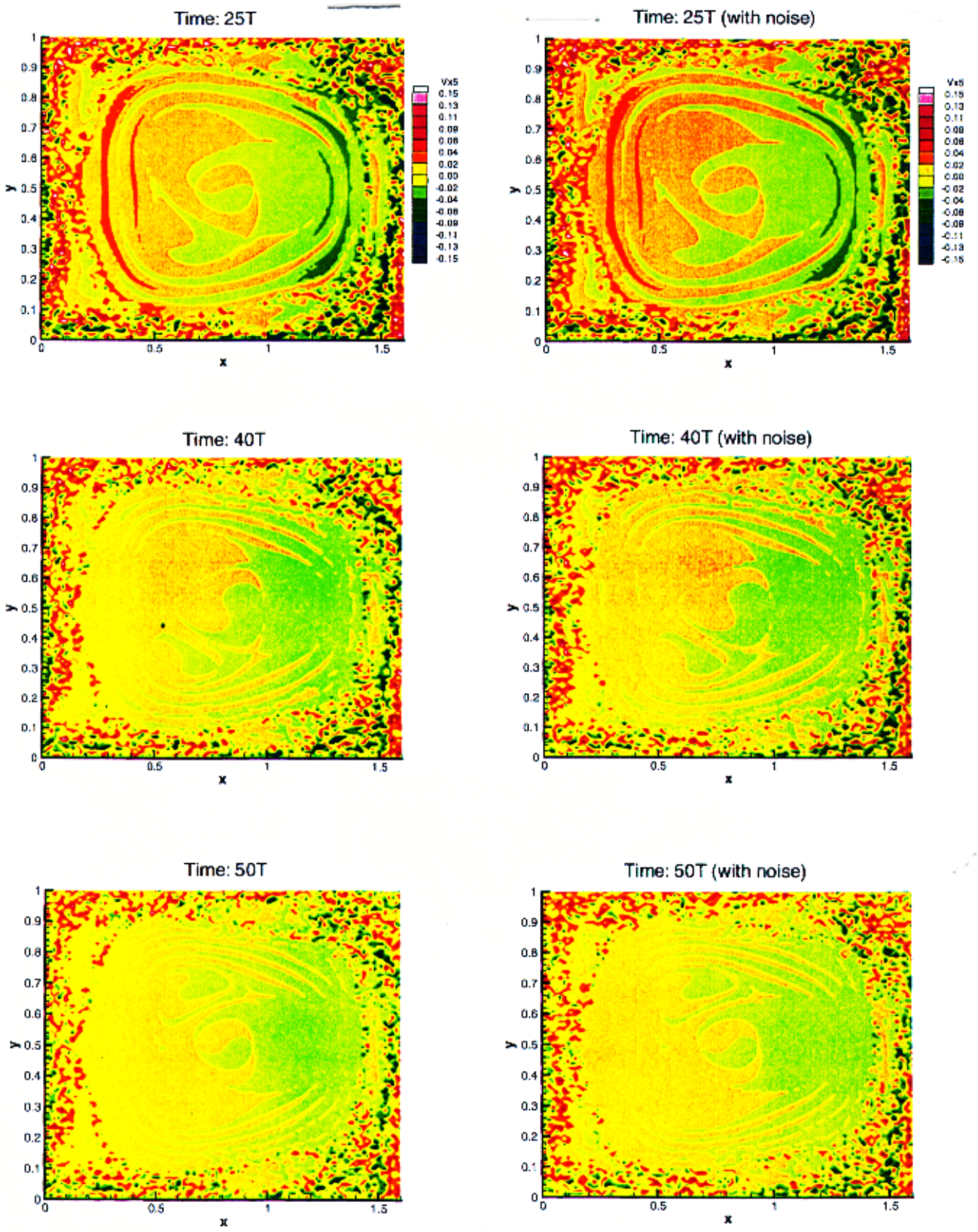

Fig. 31. Patchiness structure for cell-to-cell transport under purely periodic time-dependence (on the left) and with random perturbations (with $\nu = 10^{-4}$) added in the velocity field. The cell parameters are set at $A = 0.5$, $\varepsilon\gamma = 0.2$, $\omega = 4.2$, $\delta = \pi$, $T = 1.496$, and $dt = 10^{-3}$.

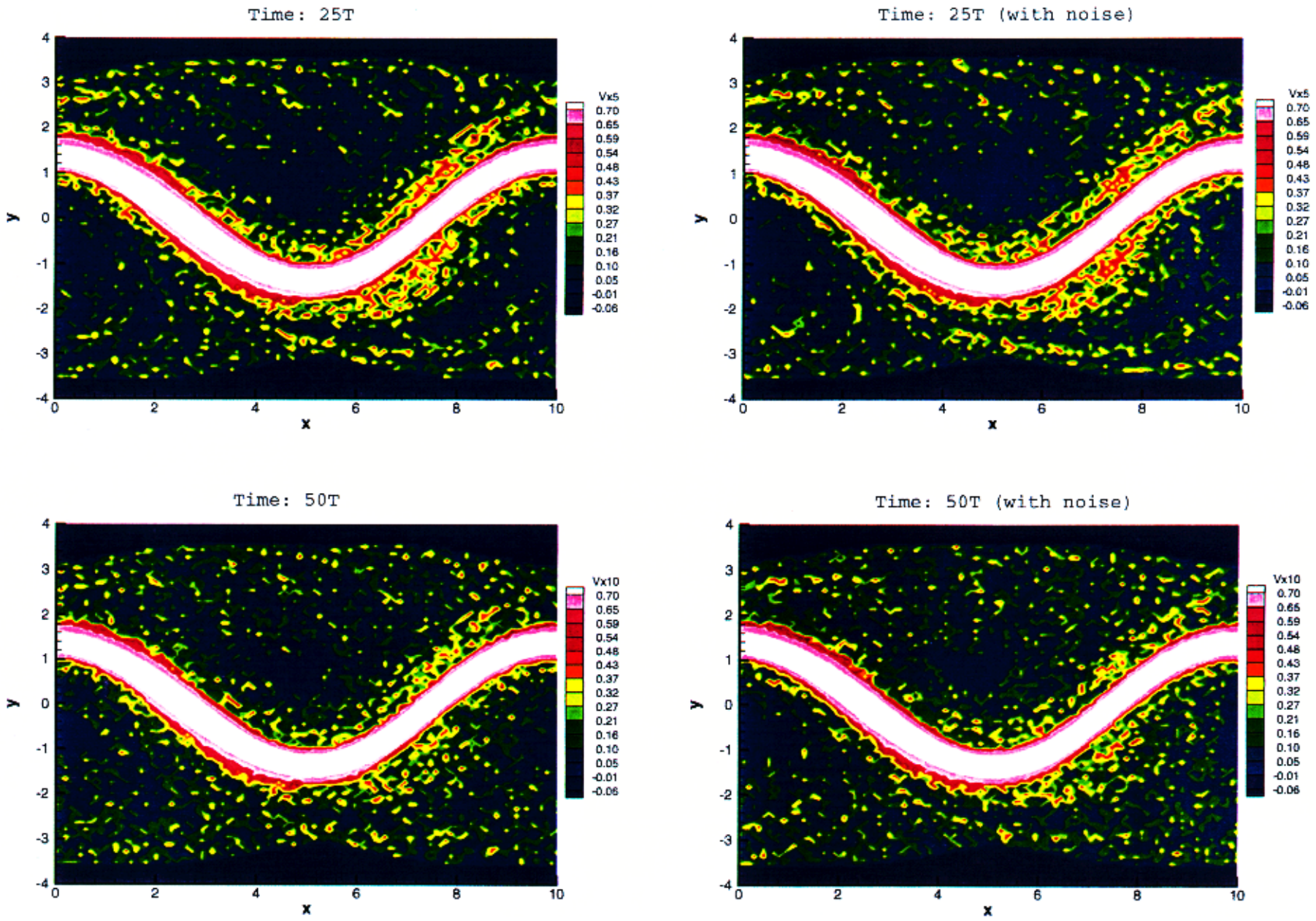

Fig. 32. Patchiness structure for jet transport under periodic time-dependence (on the left), and with a random component in the velocity field (on the right). The jet parameters are the same as Fig. 14 and $\varepsilon\gamma = 0.2$, $\omega = 0.3$, $T = 20.94$, and $dt = 0.01$.

high probability of drifting towards the central jet region, and thus the associated average x-velocity values increase.

6. Discussion

We have presented an extensive numerical study of geometrical and statistical properties of particle motion in flows representative of two different classes: Zero-mean velocity and nonzero mean velocity, and introduced a new statistical measure of nonhomogeneity of a flow that we call dispersion of patchiness. In the case of zero-mean flows, we have studied a model of Rayleigh–Bénard convection. In this case, for larger amplitudes of perturbation the distribution of average velocities (which is actually the distribution of the particles normalized by the mean path traveled) was found to be Gaussian and the dispersion of patchiness decayed to zero as inverse of time, indicating linear in time dispersion of particles. No indication of anomalous dispersion behavior was found, although for smaller values of the amplitude of time-dependence non-Gaussian distribution of average velocities was found. In contrast, the predominating feature of distributions in the Bower–Samelson model of the meandering jet is non-Gaussianity, which is exhibited both in the existence of peaks in the distribution that correspond to regions of constant average velocity, and non-Gaussianity of parts of distributions that appear smooth. The peaks in the distribution cause Pe^2 behavior of the effective diffusivity when diffusion is introduced to the problem. The dispersion behavior without diffusion can be anomalous, but the exponent of the anomalous diffusion depends strongly on parameter values and time-scale of the study.

We conjecture that for large-scale flows the patchy distributions observed here are typical. Even with a small amount of diffusion acting, the time-scale on which the process becomes truly diffusive is very long. The further study of the structure of patches is thus necessary. A first step in that direction is taken here. We have related the formation of patches with the intersection of lobes. The statistical properties of motion are thus affected by the purely geometrical interaction of the objects in the flow. Further, the formation of resonance zones in the jet region is reflected in the statistics by the formation of a countable number of small peaks in the distribution. The addition of small diffusive noise tends to erode the isolated patchy regions much faster than the patches that are part of a larger cluster. A further study of how the addition of diffusion affects the structure of patchy regions — how different patches are mixed in a jet over long time-intervals — would be very interesting.

References

Aref, H. & El Naschie, M. S. (eds.) [1994] "Chaos applied to fluid mixing," *Chaos, Solitons & Fractals* **4**(6), 1–380.

Arnold, V. I. & Avez, A. [1968] *Ergodic Problems in Classical Mechanics* (W. A. Benjamin, New York).

Babiano, A., Provenzale, A. & Vulpiani, A. (eds.) [1994] *Chaotic Advection, Tracer Dynamics, and Turbulent Dispersion*, Proc. NATO Advanced Research Workshop and EGS Topical Workshop on Chaotic Advection, Conf. Centre Sereno di Gavo, Italy, 24–28 May 1993; *Physica* **D76**, 1–329.

Beigie, D., Leonard, A. & Wiggins, S. [1994] "Invariant manifold templates for chaotic advection," *Chaos, Solitons & Fractals* **4**(6), 749–868.

Bower, A. S. [1991] "A simple kinematic mechanism for mixing fluid parcels across a meandering jet," *J. Phys. Oceanogr.* **21**(1), 173–180.

Camassa, R. & Wiggins, S. [1991] "Chaotic advection in a Rayleigh–Bénard convection, *Phys. Rev.* **A43**(2), 774–797.

Chandrasekhar, S. [1943] "Stochastic problems in physics and astronomy," *Rev. Mod. Phys.* **15**(1), 1–89.

Chandrasekhar, S. [1961] *Hydrodynamics and Hydromagnetic Stability* (Dover, New York).

Crisanti, A., Falcioni, M., Vulpiani, A. & Paladin, G. [1991] "Lagrangian chaos: Transport, mixing and diffusion in fluids," *Rivista Del Nuovo Cimento* **14**(12), 1–80.

Duan, J. & Wiggins, S. [1996] "Fluid exchange across a meandering jet with a quasi-periodic variability," *J. Phys. Oceanogr.* **26**(7), 1176–1188.

Malhotra, N. & Wiggins, S. [1998] "Geometric structures, lobe dynamics, and Lagrangian transport in flows with aperiodic time-dependence, with applications to Rossby wave flow," *J. Nonlinear Sci.* **8**, 401–456.

Mezić, I. [1994] "On the geometrical and statistical properties of dynamical systems: Theory and applications," Caltech PhD thesis.

Mezić, I. & Wiggins, S. [1995a] "On the dynamical origin of asymptotic t^2 dispersion of a nondiffusive tracer in incompressible laminar flows," *Phys. Fluids* **6**(6), 2227–2229.

Mezić, I. & Wiggins, S. [1995b] "On the dynamical origin of asymptotic t^2 dispersion of a nondiffusive tracer in incompressible laminar flows," *Phys. Rev.* **E52**(6), 3215–3217.

Mezić, I., Brady, J. F. & Wiggins, S. [1996] "Maximal effective diffusivity for time periodic incompressible fluid flows," *SIAM J. Appl. Math.* **56**(1), 40–56.

Parker, T. S. & Chua, L. O. [1989] *Practical Numerical Algorithms for Chaotic Systems* (Springer-Verlag, Berlin).

Pasmanter, R. [1991] "Anomalous diffusion and Patchiness generated by Lagrangian chaos in shallow tidal flows," *Phys. Fluids* **3**(5), 1441.

Pasmanter, R. [1988] "Anomalous diffusion and anomalous stretching in vortical flows," *Fluid Dyn. Res.* **3**, 320–326.

Samelson, R. M. [1992] "Fluid exchange across a meandering jet," *J. Phys. Oceanogr.* **22**(4), 431–440.

Shlesinger, M. F., Zaslavsky, G. M. & Frisch, U. (eds.) [1994] *Lévy Flights and Related Topics in Physics*, Lecture Notes in Physics **450** (Springer-Verlag, New York).

Solomon, T. H. & Gollub, J. P. [1988] "Chaotic particle transport in time-dependent Rayleigh–Bénard convection," *Phys. Rev.* **A38**, 6280–6286.

Wiggins, S. [1992] *Chaotic Transport in Dynamical Systems*, Interdisciplinary Applied Mathematical Sciences Series (Springer-Verlag).